HHS Public Access

Author manuscript

Nat Neurosci. Author manuscript; available in PMC 2022 January 27.

Published in final edited form as:

Nat Neurosci. 2021 March ; 24(3): 368–378. doi:10.1038/s41593-020-00771-8.

The S1 protein of SARS-CoV-2 crosses the blood–brain barrier in mice

Elizabeth M. Rhea[1,2], **Aric F. Logsdon**[1,2], **Kim M. Hansen**[1], **Lindsey M. Williams**[1], **May J. Reed**[1,2], **Kristen K. Baumann**[1], **Sarah J. Holden**[3], **Jacob Raber**[3,4], **William A. Banks**[*,1,2], **Michelle A. Erickson**[1,2]

[1]Geriatrics Research Education and Clinical Center, Veterans Affairs Puget Sound Health Care System, Seattle, WA USA

[2]Division of Gerontology and Geriatric Medicine, Department of Medicine, University of Washington School of Medicine, Seattle, WA USA

[3]Department of Behavioral Neurosciences, Oregon Health & Science University, Portland, OR USA

[4]Department of Neurology, Psychiatry, and Radiation Medicine; Division of Neuroscience, Departments of Neurology and Radiation Medicine, ONPRC, Oregon Health & Science University, Portland, OR USA

Abstract

It is unclear whether SARS-CoV-2, which causes COVID-19, can enter the brain. SARS-CoV-2 binds to cells via the S1 subunit of its spike protein. We show that intravenously injected radioiodinated S1 (I-S1) readily crossed the blood-brain barrier (BBB) in male mice, was taken up by brain regions and entered the parenchymal brain space. I-S1 was also taken up by lung, spleen, kidney, and liver. Intranasally administered I-S1 also entered the brain, though at ~10 times lower levels than after intravenous administration. *APOE* genotype and sex did not affect whole-brain I-S1 uptake, but had variable effects on uptake by the olfactory bulb, liver, spleen, and kidney. I-S1 uptake in the hippocampus and olfactory bulb was reduced by lipopolysaccharide-induced inflammation. Mechanistic studies indicated that I-S1 crosses the BBB by adsorptive transcytosis, and that murine angiotensin-converting enzyme-2 is involved in brain and lung uptake, but not in kidney, liver, or spleen uptake.

[*]Corresponding author: WAB, 1/810C, 1660 S Columbian Way, Seattle, WA 98108 Phone: 206 764 2701, wabanks1@uw.edu.

Author Contributions:

EMR: experimental design, experimental work and data analysis (mouse experiments) writing, editing, graphics
AFL: writing, editing, experimental work and data analysis (mouse experiments)
KMH: writing, editing, experimental work and data analysis (protein labeling and characterization, mouse experiments)
LMW: experimental work and data analysis (in vitro studies), writing, editing.
MJR: experimental work (mouse experiments), experimental design, writing, editing
KKB: experimental work (mouse experiments), writing, editing
SJH: experimental work (APOE mouse husbandry), writing, editing
JB: writing, editing, experimental design
WAB: experimental design, statistics, writing, editing, graphics
MAE: writing, editing, experimental design, experimental work (protein labeling, mouse experiments, in vitro studies)

Competing interests: The authors declare no competing interests.

Introduction

Severe acute respiratory syndrome corona virus 2 (SARS-CoV-2) is responsible for the COVID-19 pandemic. In addition to pneumonia and acute respiratory distress, COVID-19 is associated with a host of symptoms that relate to the central nervous system (CNS), including loss of taste and smell, headaches, twitching, seizures, confusion, vision impairment, nerve pain, dizziness, impaired consciousness, nausea and vomiting, hemiplegia, ataxia, stroke, and cerebral hemorrhage[1, 2]. It has been postulated that some of the symptoms of COVID-19 may be due to direct actions of the virus on the CNS; for example, respiratory symptoms could be in part due to SARS-CoV-2 invading the respiratory centers of the brain[1, 3]. Encephalitis has also been reported in COVID-19, and could be a result of virus or viral proteins having entered the brain[4, 5]. SARS-CoV-2 mRNA has been recovered from the cerebrospinal fluid[4], suggesting it can cross the BBB. Other coronaviruses, including the closely related SARS virus that caused the 2003–4 outbreak, are able to cross the BBB[6–8] and SARS-CoV-2 can infect neurons in a brainsphere model[9]. However, SARS-CoV-2 could induce changes in the CNS without directly crossing the BBB, as COVID-19 is associated with a cytokine storm, and many cytokines cross the BBB to affect CNS function[10].

Here we assess whether one viral protein of SARS-CoV2, the spike 1 protein (S1), can cross the BBB. This question is important and clinically relevant for two reasons. First, some proteins shed from viruses have been shown to cross the BBB, inducing neuroinflammation and otherwise impairing CNS functions[11–17]. Second, the viral protein that binds to cells can be used to model the activity of the virus; in other words, if the viral binding protein crosses the BBB, it is likely that protein enables the virus to cross the BBB as well[18, 19]. S1 is the binding protein for SARS-CoV-2[20]; it binds to angiotensin converting enzyme 2 (ACE2)[21–23] and probably other proteins as well.

In this study, we show that radioiodinated S1 (I-S1) readily crossed the murine BBB, entered the parenchymal tissue of brain and, to a lesser degree, was sequestered by brain endothelial cells and associated with the brain capillary glycocalyx. We describe I-S1 rate of entry into the brain after intravenous and intranasal administration, determined its uptake in 11 different brain regions, examined the effect of inflammation, *APOE* genotype, and sex on I-S1 transport, and compared I-S1 uptake in the brain to the uptake in liver, kidney, spleen, and lung. Based on experiments with the glycoprotein wheatgerm agglutinin, we found that brain entry of I-S1 likely involves the vesicular-dependent mechanism of adsorptive transcytosis.

Results

I-S1 protein is transported across the mouse BBB

We obtained S1 proteins from two commercial sources, RayBiotech and AMSBIO. The S1 proteins were radiolabeled in-house, and verified to be intact post-labeling by autoradiography gels (Extended Figure 1 and Supplemental Figure 1). We determined whether intravenously injected I-S1 could cross the BBB in mice, by measuring its blood-to-

brain influx constant (Ki) using multiple-time regression analysis (MTRA). MTRA plots the tissue/serum ratios for I-S1 against exposure time, which is a measure of time that has been corrected for the clearance of I-S1 from blood. The slope of the linear portion of this plot measures Ki, i.e. the unidirectional influx constant for I-S1.

We co-injected ^{99m}Tc – labeled albumin (T-Alb) along with the I-S1. T-Alb crosses the intact BBB poorly and so can be used to measure the vascular space of the brain. Any brain/serum ratios for I-S1 that exceed the brain/serum ratios of T-Alb therefore represent extravascular I-S1; that is, material which has crossed the BBB. T-Alb can also be used to measure the leakiness of peripheral tissue beds and of a BBB that has been disrupted by disease or inflammation.

The blood-to-brain influx constants (Ki's) of the I-SI proteins from the two sources differed by about 3% (Figure 1). These results show that unlike T-Alb, I-S1 readily crosses the mouse BBB.

I-S1 is cleared from blood and taken up by peripheral tissues

We determined the clearance of intravenously injected I-S1 from RayBiotech from blood and its uptake in brain and other tissues, again using MTRA (Figure 2). Clearance of I-S1 from blood was linear for the first 10 min, with a half-time clearance of about 6.6 min (Figure 2A), and a plateau after that. In Figure 2 (and in subsequent figures), tissue/serum ratios for T-Alb were subtracted from the tissue/serum ratios for I-S1. These "delta" tissue/serum ratios were thus corrected for the I-S1 in the vascular space and for any I-S1 that would have entered tissue because of a leaky capillary bed. The resulting delta values thus represent specific uptake of I-S1 by the tissues.

All tissues showed uptake of I-S1 (Figure 2B–F). Spleen and liver uptake was nonlinear, suggesting that their tissue beds were coming into equilibrium with blood. Most substances in blood are cleared by kidney or liver; the much higher I-S1 uptake in liver compared to kidney suggests that I-S1 is cleared from blood predominantly by the liver. To determine if there were regional differences in brain uptake, we collected the olfactory bulb and dissected the whole brain into 10 regions (Extended Data Figure 2). We found that I-S1 entered all brain regions, with no statistically significant differences among them.

We similarly determined the clearance of I-S1 (AMSBIO) from blood and its uptake by brain and other tissues (Figure 3). The results were similar to those obtained with I-S1 derived from RayBiotech (Figure 2), but there were a few differences. The AMSBIO-derived I-S1 was cleared from blood faster (half-life of 3.6 min) and the rate of liver uptake was nearly 5 times faster than liver uptake of RayBiotech-derived I-S1 ($p<0.0001$). Together, these results show that I-S1 is cleared from blood primarily by the liver and that S1 has access to other tissues relevant for COVID-19, including kidney, lung, and spleen.

I-S1 is stable in brain and blood

We measured the stability of intravenously injected I-S1 from RayBiotech in blood and brain through acid precipitation (Supplementary Table 1). I-S1 added to tissues (processing controls) ex vivo showed little degradation. Radioactivity recovered from brain 10 min after

intravenous injection and serum 10 and 30 min after the intravenous injection of I-S1 was stable, with most of the radioactivity precipitated by acid. Radioactivity recovered from brain 30 min after the intravenous injection of I-S1 was mostly degraded. This indicates that I-S1 enters the BBB intact but is eventually degraded in the brain, although it is not clear whether this involves cleavage of the radioactive iodine from I-S1 and/or whether S1 protein itself is degraded.

Most of the I-S1 taken up by the capillary bed enters the brain parenchyma.

In rare cases, substances that seem to cross the BBB are actually sequestered by the capillary bed, which prevents them from entering the brain parenchymal/interstitial fluid space.

Therefore, we next assessed whether intravenously injected I-S1 fully crosses the capillary wall to enter brain parenchyma. For this, we used a modified version of the ‘capillary depletion’ method that also enabled us to measure the amount of intravenously injected I-S1 that is reversibly adhering to the luminal side of the capillary bed. We found that binding of I-S1 to the luminal side remained static over time, whereas there was a small increase over time in the amount of I-S1 retained by brain capillaries (Extended Figure 3). The largest change over time was the amount of I-S1 entering the parenchyma. These results show that by thirty minutes, over 50% of I-S1 has crossed the capillary wall fully to enter into the brain parenchymal and interstitial fluid spaces.

WGA enhances I-S1 uptake in brain and some peripheral tissues

Wheatgerm agglutinin (WGA) is a plant lectin that crosses the BBB through adsorptive transcytosis[24] —a process by which proteins or peptides bind to glycoproteins of the luminal surface of endothelial cells, are internalized into vesicles and then transported across the membrane. In the case of WGA, adsorptive transcytosis occurs when WGA binds to cell-surface glycoproteins containing sialic acid and N-acetylglucosamine. Many viral proteins also bind to sialic acid- and N-acetylglucosamine-containing glycoproteins, and therefore, when WGA is co-injected with such viral proteins, it enhances their transport across the BBB and uptake in peripheral tissues[18]. Here, we found that intravenously injected I-S1 (RayBiotech or AMSBIO) uptake into brain, lung, spleen, and kidney was increased compared when WGA was included in the injection (Figure 4B–E). WGA co-injection also increased clearance of I-S1 (RayBiotech), but not I-S1 (AMSBIO), as shown by a decrease in I-S1 in blood (Figure 4A). WGA co-injection decreased uptake of I-S1 (AMSBIO) but not I-S1 (RayBiotech) in the liver (Figure 4F), although it did with the WGA arm of the heparin experiment (Figure 4H).

These results strongly suggest that I-S1 crosses the BBB and peripheral tissue beds through the mechanism of adsorptive transcytosis, binding to cell surface glycoproteins that contain sialic acid or N-acetylglucosamine.

Heparin blocks uptake of I-S1 in liver but not in brain.

Some viruses use heparan sulfate on the cell membrane as a receptor[25]. Heparin can block virus uptake in tissues, presumably by binding to viral proteins and thereby blocking these viral proteins from binding to the heparan sulfate on the cell membranes[19, 26]. However, we

found that heparin co-injected with I-S1 did not affect uptake of I-S1 (RayBiotech) in brain, lung, spleen, or kidney and did not influence the effect of WGA co-injection on I-S1 uptake in these issues (data not shown). Heparin co-injected with I-S1 did block uptake of I-S1 in liver (Figure 4 H), which likely explained the observed decreased clearance of I-S1 from blood (as evidenced by the increase in I-S1 levels in serum; Figure 4G), but did not block the effects of WGA in I-S1 uptake in liver. These results indicate that I-S1 uses heparin-sensitive sites to bind to the capillary bed of the liver, but not to bind to the capillary beds of brain, spleen, lung, or kidney.

I-S1 uptake in brain was not blocked by unlabeled S1

We next determined whether transport of intravenously injected I-S1 (RayBiotech) into the brain could be blocked by including in the injection an excess of unlabeled S1 protein (AMSBIO). Unlabeled S1 did not affect brain/serum ratios for delta I-S1 at any of the tested doses (Figure 5A), although it did enhance uptake of I-S1 in lung (Figure 5C). This indicates that the binding site for I-S1 in brain tissue is not easily saturated — a characteristic of adsorptive transcytosis. Unlabeled S1 also did not affect brain/serum ratios for T-Alb (data not shown), which indicates that even the high dose of 10ug S1 did not acutely disrupt the BBB.

ACE2 likely mediates I-S1 uptake in brain and lung, but not other tissues

The ability of SARS-CoV-2 to enter cells is thought to depend on S protein binding to the membrane-bound enzyme (and glycoprotein) ACE2. To assess whether ACE2 has a role in I-S1 uptake in brain and peripheral tissue, we intravenously co-injected ACE2 or the ACE2 substrates AngII and ghrelin with I-S1 (RayBiotech). This did not affect blood levels of intravenously injected I-S1 or T-Alb (data not shown), indicating that these proteins did not affect the volume of distribution or clearance of either S1 or albumin. Co-injection of ACE2 increased kidney levels of intravenously injected T-Alb: $F(4,36) = 2.63$, $p = 0.0505$; vehicle: 119 ± 4.4 μL/g (n = 8 mice); ACE2: 151 ± 15.6 μL/g (n = 8 mice), $p = 0.02$), possibly indicating that ACE2 affects renal clearance of albumin. Only ACE2 co-injection enhanced I-S1 uptake in brain (Figure 5B). Uptake in lung was increased by co-injection of S1, ghrelin or ACE2, but not angiotensin II (Figure 5C), whereas uptake in liver, kidney, or spleen was not altered by co-injection of any of these substances (data not shown). These results suggest that ACE2 is involved in S1 uptake in lung and probably brain, but not for I-S1 uptake in spleen, liver, or kidney.

Inflammation increases I-S1 uptake in brain and lung

Since SARS-CoV-2 infection induces an inflammatory state, we next determined whether an inflammatory state — in this case, induced by LPS injection — affects uptake of intravenously injected I-S1 (RayBiotech) in brain and peripheral tissues. Mice received a 3mg/kg injection of LPS derived from *Salmonella typhimurium* (Sigma, St. Louis, MO) at t = 0 and again 6 and 24 h later and received an intravenous I-S1 or T-Alb injection 28 h after the first LPS injection; this LPS regimen can disrupt the BBB, increase its permeability to viruses and viral proteins[27, 28], and increase the blood level of many of the cytokines found to be elevated in the cytokine storm associated with COVID-19[5, 29].

We found that LPS did not affect T-Alb blood levels, indicating that inflammation did not induce volume contraction of the vascular space nor leakiness of the peripheral capillary beds in these mice. Mice that had received LPS did have higher I-S1 serum levels (Figure 6A), indicating a decrease in clearance from blood (likely because of the decreased I-S1 uptake in liver observed in these mice (Figure 6B)), as well as higher T-Alb brain/serum ratios, indicating BBB disruption [control: 8.52 ± 0.19 μL/g (n = 10); LPS: 12.2 ± 0.68 μL/g (n = 8), t = 5.74, p<0.0001]. These mice also had higher I-S1 brain/serum ratios (i.e. ratios not corrected for I-S1 in the vascular space and for any I-S1 brain entry due to leakage), indicating increased I-S1 passage across the BBB [Control: 12.06 ± 0.26 μL/g (n = 10); LPS: 14.9 ± 0.64 μL/g (n =8), t = 4.38, p = 0.0005], although their delta brain/serum ratios for I-S1 (i.e. corrected ratios) were not different from controls (except in the olfactory bulb) (Figure 6C). The only tissue showing an increased uptake of I-S1 after receiving LPS was the lung, which increased 101% (Figure 6B). These results show that inflammation could increase S1 toxicity for lung by increasing its uptake. The results also show that in mice, inflammation can increase intravenously injected I-S1 entry into brain, but this is likely due to BBB disruption rather than by enhancing absorptive transcytosis.

I-S1 enters brain and blood after nasal administration

Some viruses can enter the brain via the olfactory nerve, a cranial nerve with projections through the cribriform plate[30]. Other viruses may cross the BBB after entering the blood stream from the nasal compartment. It is unclear whether SARS-CoV-2 in the nose can enter brain by either of these routes. We therefore assessed the ability of intranasally administered I-S1 to enter brain. Following a 1μL vehicle solution containing I-S1 to each naris at the level of the cribriform plate (where the olfactory nerve emerges from the cranial vault) I-S1 was detected in all brain regions (Figure 7A–B). I-S1 levels in whole brain, frontal cortex, cerebellum, midbrain, and pons-medulla were higher at 30 min compared to 10 min post administration. I-S1 distribution in the brain was mostly homogenous, although levels in the olfactory bulb and hypothalamus were higher than in other brain regions at 10 min and, in the olfactory bulb also at 30 min post-administration. Whole-brain I-S1 levels expressed as the percent of the administered dose were about 10 times higher after intravenous injection than after intranasal injection (Figure 7A). Radioactivity appeared in blood after intranasal administration of I-S1, indicating that some I-S1 had entered the blood stream (data not shown). The AUC for I-S1 in blood after intranasal administration was 9.42 (%Inj/ml)-min, whereas the AUC for I-S1 in blood after iv injection was 1430 (%Inj/ml)-min, indicating that the bioavailability for the nasal route is 0.66%. Together, these results show that I-S1 can enter the brain and distribute in a time-dependent manner to all brain regions after intranasal administration. However, I-S1 uptake in the brain via this route is much less efficient than uptake after transport across the BBB.

Effects of sex and APOE genotype on I-S1 uptake.

Male sex and *APOE4* genotype in comparison to the *APOE3* genotype are risk factors for both contracting and having a poor outcome to COVID-19[31–33]. Therefore, we determined uptake of intravenously injected I-S1 (RayBiotech) or T-Alb in male and female mice expressing human *APOE3* or *APOE4* under the expression of the mouse *Apoe* promoter. *APOE* genotype and sex did not affect T-Alb brain/serum ratios (Figure 8A). Two-way

ANOVA showed an effect of sex on I-S1 uptake in olfactory bulb and spleen and an effect of *APOE* genotype on I-S1 uptake in liver, spleen, and kidney (Figure 8B–H). Multiple comparisons tests showed that in comparison to the other three groups male mice expressing human *APOE3* had the fastest I-S1 uptake of I-S1 in olfactory bulb liver, and kidney, whereas in comparison to the other three groups female mice expressing human APOE3 has the fastest I-S1 uptake in spleen. These results suggest that enhanced uptake of I-S1 by some tissues could contribute to the increased risk of COVID-19 associated with being male, but not to the risk associated with the *APOE4* genotype.

I-S1 transport across an in vitro model of the BBB

To determine whether the I-S1 crosses endothelial-like cells in an *in vitro* model of the human BBB, we compared transport of I-S1 vs T-Alb across monolayers of human iPSC-derived brain endothelial-like cells (iBECs) seeded on transwells. Three independent experiments showed that rate of passage of I-S1 (RayBiotech) in the luminal-to-abluminal direction was not statistically significant when compared to that of T-Alb (Extended Data Figure 4A). One experiment indicated that unlabeled S1 did not inhibit I-S1 (RayBiotech) passage (Extended Data Figure 4B). WGA also had no effect on RayBiotech I-S1 transport (Extended Data Figure 4C). I-S1 (RayBiotech) had a significantly higher permeability coefficient than I-S1 (AMSBIO I-S1) *in vitro* (Extended Data Figure 4D); however this difference was not significant after correcting for T-Alb transport. In summary, these results suggest that iBECs may be more permeable to I-S1 than to T-Alb, but the difference is too small to support mechanistic studies using this model.

Discussion

The results from this study show that I-S1 from two different commercial sources readily crosses the mouse BBB, at least when injected intravenously. I-S1 was taken up by all 11 brain regions examined. Such widespread entry into brain of I-S1 could explain the diverse effects of S1 and/or SARS-CoV-2 such as encephalitis, respiratory difficulties, and anosmia[1, 3, 4]. S1 is the SARS-CoV-2 protein that initially binds to cell-surface receptors, setting the stage for viral internalization. In terms of transport across the BBB, viral binding proteins often behave similarly to the virus itself. For example, interactions (including binding and transport) between the HIV-1 glycoprotein gp120 and the BBB are similar to those for the complete virus[18, 28]. Additionally, many if not most viral proteins themselves can be biologically highly active; for example, gp120 is highly toxic[11–17]. Coronavirus spike proteins are often cleaved from the virus by host cell proteases. Once cleaved, coronavirus spike S1 and S2 subunits are not held covalently by disulfide bonds and so S1 could be shed from virions[34]. It is possible that during infection by SARS-CoV-2, shed S1 is available to cross the BBB, triggering responses in the brain in itself, without necessarily involving crossing of intact virus particles. Thus, determining whether S1 crosses the BBB is important for understanding whether SARS-CoV-2 and S1 itself could induce neurotoxicity.

Our method of studying S1 pharmacokinetics has many advantages over the more traditional approach of determining viral uptake and distribution that is based on virus recovery. Radioactive labeling allows S1 to be detected at very low levels and quantification of the

rates of uptake for brain and other tissues. Factors that might affect viral protein uptake can be manipulated experimentally in healthy, rather than infected, animals. Recovery of I-S1 from a tissue reflects only factors related to permeability, whereas recovery from infected mice also reflects other factors, such as rate of virus replication in that tissue.

A crucial question which we partially answered here was: what receptor does I-S1 use to enter brain and other tissues? Based on experience with SARS, it has been assumed that SARS-CoV-2 will bind to human ACE2, but not murine ACE2. SARS can infect WT mice, but doesn't produce severe symptoms and death, except in transgenic mice overexpressing human ACE2[35] - although this could also simply be due to the fact that these transgenic mice express 8–12 times more ACE2 than WT mice. The mice we used here only expressed murine receptors and so the assumption that ACE2 must be the human protein is clearly wrong; this demonstrates that WT mice can be used in kinetics studies of S1 and probably SARS-CoV-2.

We did find reasonably strong evidence that murine ACE2 is involved in I-S1 uptake in lung, as co-injection of I-S1 with soluble ACE2 and ACE2 substrates increased the uptake of I-S1 (the perhaps surprising observed increase rather than decrease is discussed further below). The evidence for ACE2 involvement in brain I-S1 uptake is weaker than that for lung, as here, uptake was affected by co-injection with soluble ACE2, but not by ACE2 substrates. The finding that I-S1 uptake in kidney, liver, and spleen were unaffected by soluble ACE2 or by ACE2 substrates indicate that receptors other than, or in addition to, ACE2 are involved in uptake of I-S1 in some tissues.

That S1 and even SARS-CoV-2 would use more than one receptor is not surprising when one considers that many viruses use multiple receptors. For example, HIV-1 uses the CD4 and mannose-6 phosphate receptors, and the rabies virus uses the acetylcholine receptor, a nerve growth factor receptor, and the neural cell adhesion molecule to enter cells[25, 36]. Receptors (besides ACE2) that can bind or are predicted to bind SARS-CoV-2 based on modeling include basigin, cyclophilins, dipeptidyl peptidase-4[37, 38] and GRP78[39].

One reason that a virus can use such a diversity of receptors is that viruses bind with less specificity than do endogenous receptor ligands. The binding sites for viral proteins are often highly charged regions on the cell-membrane glycoprotein owing to high concentrations of sialic acid, N-acetylglucosamine, or heparan sulfate. Coronaviruses in general bind to glycoproteins high in sialic acid[40]. Pioneering work showed that WGA binding to BBB regions rich in sialic acid or N-acetylglucosamine resulted in WGA being transported across the BBB through the mechanism of adsorptive transcytosis[24]. WGA co-administered with a weaker inducer of adsorptive transcytosis will often increase rather than block the BBB penetration of the weaker inducer[41]. In the current study, the ability of WGA to increase the I-S1 uptake in brain suggests that S1 crosses the BBB through adsorptive transcytosis.

Because the spike protein of SARS-CoV-2 is more highly charged than the spike protein of SARS, it has been suggested that it may bind to a larger number of receptors[42]. Some viruses bind receptors rich in heparan sulfate; uptake of those viruses is inhibited by heparin[25]. We showed that I-S1 uptake in liver was inhibited by heparin, but uptake in

brain and other peripheral tissues was not. These results show that S1 uses heparan sulfate to bind to liver but not to other tissues. We conclude that it is likely that a number of receptors are involved in S1 uptake; which receptor is most important varies from tissue to tissue. It will be important to identify the membrane-bound glycoproteins that serve as receptors for SARS-CoV-2.

It is unclear why, in our study, co-injection with ACE2 or ACE2 substrates enhanced rather than inhibited uptake of intravenously injected I-S1, but there are some possible explanations. Since S1 does not bind to the ACE2 catalytic site[43,42], traditional ligand–receptor dose-dependent inhibition kinetics may not occur. The ACE2 we co-injected with I-S1 may have bound circulating AngII that would normally have competed with I-S1 for binding to membrane-bound ACE2. In addition, S1 is attached to SARS-CoV-2 as a homotrimer[38], but we studied monomeric S1; it is possible that co-injection of ACE2 ligands altered ACE2 conformation in such a way that it facilitates binding of S1 monomer.

Risk factors for both contracting COVID-19 and having a poor outcome are being male and being ApoE4 positive in comparison to ApoE3 positive[31–33], whereas cytokine storm is a characteristic of severe disease[44]. We found that the influence of sex, ApOE genotype and inflammatory state on I-S1 uptake varied among the tissues. Sex and human ApoE status in mice did not affect uptake of intravenously injected I-S1 in whole brain or lung, but did affect its uptake in olfactory bulb, liver, spleen, and kidney, with higher uptake in males. This suggests that some of the risk of poor outcome for males may be related to the degree to which their tissues have an enhanced uptake of S1 or SARS-CoV-2. However, ApoE3, not ApoE4, was associated with a higher uptake rates of I-S1 by olfactory bulb, liver, spleen, and kidney, suggesting that the risk associated with ApoE status is unlikely to be due to increased S1 or SARS-Cov-2 tissue uptake.

Inflammation induced by LPS injection increased the amount of intravenously injected I-S1 entering brain, but this increase was likely due to BBB disruption and not due to enhancement of adsorptive transcytosis; indeed, uptake of I-S1 after correction for BBB disruption was actually lower in one brain region, the olfactory bulb. LPS-exposed mice had higher I-S1 uptake in lung but lower uptake in spleen and liver; the latter likely explains why these mice had reduced I-S1 clearance from blood. Notably, this decrease in clearance from blood observed in mice in an inflammatory state suggests that all tissues will be exposed to higher S1 levels than in the non-inflammatory state.

A lethal infection can occur after intranasal administration of SARS[35]. It has been postulated that nasal virus spreads to the lung and from there to blood and brain[35], but others suggest that SARS-CoV-2 in the nares could spread to brain by way of olfactory nerve[45], as do many other viruses[30]. Although our findings show that intranasally administered I-S1 is able to enter mouse brain, they suggest the BBB is the major route for I-S1 entry into brain. Moreover, a very small amount (0.66% bioavailability after intranasal administration) of I-S1 was found in blood, suggesting poor nasal-to-blood transfer. However, our studies were designed to assess the ability of I-S1 to enter brain by way of the olfactory nerve and not to assess its ability to enter the blood by way of nasal vasculature. Nevertheless, our results

favor some site other than the nares, such as lung, as being the entry point of S1 detected in blood.

It is important to note that although the study shows that I-S1 crosses the BBB in mice, this may not be the case in humans. For that reason, we used *in vitro* models of the human BBB, which can be useful in studying mechanisms of BBB permeability. The model used in this study is derived from human iPSCs and develops a brain-endothelial cell-like phenotype that includes functional BBB influx and efflux transporters and strong barrier properties that permit the study of transport without confounding effects of high baseline leakage[46, 47]. In this model, we did not observe significant differences in permeability for I-S1 vs T-Alb. The apparent absence of I-S1 transport across the BBB in this in vitro model could be due to technical issues, such as blockers of I-S1 binding in the buffers. It could also mean that the iBECs did not express the cell-membrane glycoproteins necessary for I-S1 transport, or it could mean that I-S1 is not able to cross the human BBB. A note of caution with regard to the validity of using monomeric S1 as a model for SARS-CoV-2 is that S1 is normally attached to SARS-CoV-2 as a trimer. However, the S1 protein may be shed from the virus in vivo, and studying S1 monomers therefore may have validity by itself – although there is currently no direct evidence that spike proteins are shed from SARS-CoV-2. Altogether, our results do strongly suggest that the S1 protein is able to cross the murine BBB through a mechanism resembling adsorptive transcytosis and to be taken up by peripheral tissues independently of human ACE2.

Methods

Mice

All mouse studies were approved by the local IACUC at OHSU and the VA Puget Sound Healthcare System and conducted in AAALAC approved facilities. Male CD-1 mice (6–10 weeks old) were purchased from Charles River Laboratories (Hollister, CA). A total of 204 CD-1 males were used for all studies. Human E3- and E4-targeted replacement (TR) male and female mice, generated as described[48], were bred at the Oregon Health & Sciences University (OHSU) prior to transfer to the Veterans Affairs Puget Sound Health Care System (VAPSHCS) for the experiments of this study. E3 and E4 TR mice were approximately 4 months of age on the day of the study. A total of 21 E3 and 20 E4 TR mice were used for all studies. Mice had *ad libitum* access to food and water and were kept on a 12/12 hour light/dark cycle. Temperature was maintained at 18–23°C and humidity was maintained at 40–60%. For all experiments, mice were anesthetized with an intraperitoneal (ip) injection of 0.15–0.2 mL of 40% urethane to minimize pain and distress. Anesthetized mice were placed on a heating pad until time of use. At the end of each study, mice were euthanized by decapitation while under anesthesia.

Sources and radioactive labeling of proteins

The S1 proteins were provided by the manufacturers (RayBiotech, Cat no 230–30161, Peachtree Corners, GA, Val16-Gln690; AMSBIO, AMS.S1N-C52H3, Abingdon, UK, Val16-Arg685). The proteins were dissolved in phosphate buffered saline (PBS, pH 7.4) at a concentration ranging from 0.45–0.61 mg/mL. The proteins were produced in HEK293

cell lines, had C-terminal His tags, were calculated to be about 76 kDa in protein, but migrated on gel at 100–120 kDa because of glycosylation. Upon receipt, the S1 proteins were thawed and aliquoted into 5μg portions, and either used immediately or stored at −80 °C until use. The 5 μg of thawed S1 protein was radioactively labeled with 1 mCi ^{125}I (Perkin Elmer, Waltman, MA) using the chloramine-T method, as described[49]. The radioiodinated S1 (I-S1) was purified on a column of G10 Sephadex (GE Healthcare, Uppsala, SE) and eluted with phosphate buffer (PB) into glass tubes containing 1% bovine serum albumin in lactated Ringer's solution (BSA-LR). We estimated based on the amount of protein iodinated that the specific activity of I-S1 to be approximately 11 Ci/g or about 12.5 ng/300,000 cpm. Bovine serum albumin (Sigma, St. Louis, MO) was labeled with ^{99m}Tc (GE Healthcare, Seattle, WA) using the stannous tartrate method[50]. The ^{99m}Tc – labeled albumin (T-Alb) was purified on a column of G-10 Sephadex. Both of the I-S1's and the T-Alb were more than 90% acid precipitable. The molecular weight of the labeled proteins was confirmed by running 200,000–600,000 CPM activity in 1x LDS buffer (Invitrogen) with or without reducing agent (Invitrogen) on a 4–12% bis-tris gel (Genescript) in 3-(N-morpholino)propanesulfonic acid (MOPS) buffer (Invitrogen). The gel was then fixed for 30 min in 10% acetic acid/50% methanol, washed 3x with water, and then dried using a DryEase® Mini-Gel Drying System (Invitrogen). Dried gels were exposed on autoradiography film for 24 hours and then developed. Major bands of I-S1 from RayBiotech and AMSBIO migrated at their predicted molecular weight patterns, based on manufacturer data (Extended Data Figure 1).

Measurement of blood-to-brain entry rate (Ki)

Multiple-time regression analysis (MTRA)[51, 52] was used to measure the unidirectional blood-to-brain influx constant (Ki) for I-S1. In anesthetized mice, the left jugular vein was exposed for an intravenous (iv) injection of 0.1 mL BSA-LR containing 3×10^5 cpm of I-S1. T-Alb (6×10^5 cpm) was also included in the injection for measurement of the vascular space for the brain and the albumin space for peripheral tissues. At time points between 1 and 30 min, blood was collected from the carotid artery. Blood was centrifuged at 3200×g for 10min and 50uL serum was collected. The whole brain, kidney, and spleen and portions of the lung and liver were removed and weighed. Tissues and serum were placed into a Wizard 2 gamma counter (Perkin Elmer), and the levels of radioactivity were measured. Results for brain and other tissues were expressed as the tissue/serum ratio in units of μL/g for both I-S1 and T-Alb. For each individual tissue, its tissue/serum ratio for T-Alb was subtracted from its tissue/serum ratio for I-S1, yielding "delta" value. These delta values were thus corrected for vascular space and any nonspecific leakage into tissue and so represent I-S1 protein uptake that was not due to trapping in the vascular space or to leakage. The delta brain/serum ratios were plotted against exposure time, a calculation that corrects for clearance from blood:

$$\text{Expt} = \left[\int_0^t C\text{p}(\tau)\text{d}\tau\right]/\text{Cpt} \quad (1)$$

where t is the time between the iv injection and sampling, Cp is the cpm/mL of arterial serum, Cpt is the cpm/mL of arterial serum at time t, and τ is the dummy variable for time. The slope of the linear portion of the relation of tissue/serum ratio vs exposure

time measures the unidirectional influx rate (Ki in units of μL/g-min) and the Y-intercept measures Vi, the vascular space and initial luminal binding at t = 0[51, 52]:

$$\text{Tissue/serum ratio} = \text{Ki(Expt)} + \text{Vi} \quad (2)$$

Calculations of AUC and percent of injected doses

The area under the curve for the level of radioactivity in blood from 0–30 min was calculated using Prism 8.0 software (GraphPad Inc, San Diego, CA). Results for serum were expressed as the percent of the injected dose per mL of blood (%Inj/mL). The percent of the injected dose per gram of brain (%Inj/g) was calculated by multiplying the delta brain/serum value by the %Inj/mL for I-S1.

Stability of I-S1 in brain and blood

Anesthetized mice received an injection into the jugular vein of 0.1 mL of BSA-LR containing 6×10^5 cpm of I-S1 plus 6×10^5 cpm of T-Alb. Ten minutes after the injection, arterial blood was collected from the abdominal aorta, the thorax opened and the descending thoracic artery clamped, both jugular veins severed, and 20 mL of lactated Ringer's solution perfused through the left ventricle of the heart to wash out the vascular space of the brain. The whole brain was then removed. Whole blood was centrifuged and 10 uL of serum was added to 500 uL BSA-LR and combined with an equal part of 30% tricholoroacetic acid, mixed, centrifuged, and the supernatant and pellet counted. Whole brain was homogenized in BSA-LR plus complete mini protease inhibitor (Roche, Mannheim, DE; one tab per 10 mL buffer) with a hand-held glass homogenizer, and centrifuged. The resulting supernatant was combined with equal parts of 30% trichloroacetic acid, mixed, centrifuged, and the supernatant and pellet counted. To determine the amount of degradation of I-S1 or T-Alb that occurred during processing, I-S1 and T-Alb was added to brains and arterial whole blood from animals that had not been injected with radioactivity and processed immediately as above. The percent of radioactivity that was precipitated by acid (%P) in all of these samples was calculated by the equation:

$$\%P = 100(S)/(S + P) \quad (3)$$

where S is the cpm in the supernatant and P is the cpm in the pellet.

Capillary depletion of brain

The capillary depletion method as adapted to mice was used to separate cerebral capillaries and vascular components from brain parenchyma[53, 54]. We used the variant of the technique that also estimates reversible binding to the capillary lumen. The latter is done by assessing two groups of mice, one with a vascular washout step which removes material reversibly bound to the capillary lumen (washout group) and those without the washout step (non-washout group). The difference between these groups represents material that was reversibly adhering to the capillary lumen (see equation 4 below). Mice were anesthetized and received an iv injection of 6×10^5 cpm Tc-Alb with 6×10^5 cpm I-S1 in 0.1 mL BSA-LR. 5, 10, and 30 min later, blood was obtained from the carotid artery, and the brain (non-washout group) was extracted. In a separate group of mice, blood was taken from the abdominal aorta at 5,

10, and 30 min, the thorax was opened and the descending thoracic artery clamped, both jugulars severed, and 20 mL of lactated Ringer's solution infused via the left ventricle of the heart in order to washout the vascular contents of the brain and to remove any material reversibly associated with the capillary lumen (washout group). Each whole brain was homogenized in glass with physiological buffer (10mM HEPES buffer, 141 mM NaCl, 4mM KCl, 2.8 mM $CaCl_2$, 1 mM $MgSO_4$, 1 mM NaH_2PO_4-H_2O, 10 mM D-glucose, pH 7.4) and mixed thoroughly with 26% dextran. The homogenate was centrifuged at 4255×g for 15 min at 4°C. The pellet, containing the capillaries, and the supernatant, representing the brain parenchymal space, were carefully separated. Radioactivity levels in the capillary pellet, the brain supernatant, and the arterial serum were determined for both T-Alb and I-S1 and expressed as the capillary/serum and brain parenchyma/serum ratios. The I-S1 parenchymal ratios were corrected for vascular contamination by subtracting the corresponding ratios for T-Alb; these results are reported as the delta brain parenchyma/serum ratios. The amount of S1 in the brain parenchymal space was taken as the delta brain parenchymal space from the washout group (PW), the amount in the capillary as the capillary from the washout group (CW), and the amount of material loosely binding to the luminal surface (Luminal) as:

$$\text{Luminal} = (\text{P} + \text{C}) - (\text{PW} + \text{CW}) \quad (4)$$

Where P are the delta brain parenchymal space and the capillary space, both from the nonwashout groups.

Effects of wheatgerm agglutinin (WGA) and heparin

We co-injected WGA with I-S1 to determine the role of sialic acid- and N-acetylglucosamine-containing glycoproteins in the uptake of S1 by the BBB and other tissues. Mice were anesthetized, after which the jugular vein and right carotid artery were exposed. Mice then received a jugular vein injection of 0.1 mL BSA-LR containing 3×10^5 cpm of I-S1 and 6×10^5 cpm of T-Alb and, in a subset of mice, 10 μg of the plant lectin wheat germ agglutinin (WGA, Sigma, St. Louis, MO). Brain, tissues, and serum samples were collected 5 min later and tissue/serum ratios calculated as above in units of μL/g. Heparan sulfate is used as a receptor by some viruses[25] and heparin by binding to viral proteins can block viral entry into brain[19, 26]. Therefore, separate groups of mice had heparin (12 U/mouse) included in the injection.

Saturation of I-S1 and binding to ACE2 enzyme

In anesthetized mice, the left jugular vein was exposed for an iv injection of 0.1 mL BSA-LR containing 3×10^5 cpm of I-S1 (RayBiotech) and 6×10^5 cpm of T-Alb. For some mice, the injection contained 1 μg/mouse of unlabeled S1 (AMSBIO), mouse acyl ghrelin (CBio, Menlo Park, CA), angiotensin II (Tocris, Bristol, UK), or human ACE2 (R&D, Minneapolis, MN). Ten min after iv injection, whole blood was obtained from the carotid artery and centrifuged after clotting. The whole brain, olfactory bulb, kidney, spleen, and portions of the liver and lung removed. The levels of radioactivity in the arterial serum and the tissues were determined and the results expressed as the percent of the injected I-S1 per mL for serum and delta tissue/serum ratios (μL/g) for the tissues.

Lipopolysaccharide injections

Male CD-1 mice aged 6–10 weeks were given an ip injection of 3 mg/kg LPS from *Salmonella typhimurium* (Sigma, St. Louis, MO) dissolved in sterile normal saline at 0, 6, and 24 h. At 28 h, mice were anesthetized and the left jugular vein and right carotid artery exposed. The mice were given an iv injection of 6×10^5 cpm of I-S1 and 6×10^5 cpm T-Alb in 0.1 mL of BSA/LR into the left jugular vein. Arterial blood was collected from the right carotid artery 10 min later, the mouse immediately decapitated, the brain removed, dissected into regions (olfactory bulb, frontal cortex, occipital cortex, parietal cortex, thalamus, hypothalamus, striatum, hippocampus, pons-medulla, cerebellum, midbrain), and the regions weighed. Kidney, spleen, and portions of the liver and lung were also removed and weighed. Serum was obtained by centrifuging the carotid artery blood for 10 min at 4255 ×g. Levels of radioactivity in serum, brain regions, and tissues were measured in a gamma counter. Whole brain values were calculated by summing levels of radioactivity and weight for all brain regions except for olfactory bulb. Data for brain regions from control (mice not receiving LPS) were separately analyzed for differences among brain regions and also used in comparisons with LPS treated mice. The levels of radioactivity in the arterial serum and the brain regions and tissues were determined and the results expressed as the percent of the injected I-S1 per mL for serum and delta tissue/serum ratios (μL/g) for the tissues.

Intranasal delivery of I-S1

Anesthetized mice were placed in the supine position and received a 1 μL injection of 2×10^5 – 3×10^5 cpm I-S1 in BSA/LR administered to each naris, delivered to the level of the cribriform plate (4 mm depth), using a 10 μL Multi-flex tip (Thermo Fisher Scientific, Waltham, MA). After administration, the mouse remained in the supine position for 30 s before being placed on the left side. Arterial blood was collected from the right carotid artery 10 or 30 min later, the mouse immediately decapitated, the brain removed, dissected into regions (olfactory bulb, frontal cortex, occipital cortex, parietal cortex, thalamus, hypothalamus, striatum, hippocampus, pons-medulla, cerebellum, midbrain), and the regions weighed. Serum was obtained by centrifuging the carotid artery blood for 10 min at 4255 ×g. Levels of radioactivity in serum and brain regions were measured in a Wizard 2 gamma counter. Whole brain values were calculated by summing levels of radioactivity and weight for all brain regions except for olfactory bulb. The levels of radioactivity in the arterial serum and the tissues were determined and the results expressed as the percent of the injected I-S1 per mL for serum and the percent of the injected I-S1 per g of brain region calculated.

MTRA in ApoE mice

Human APOE targeted replacement mice expressing human apoE3 or apoE4, under control of the mouse apoE promoter and on the C57BL/6J background, were provided by Dr Patrick Sullivan for breeding[55, 56], as described[57]***. With targeted replacement, the resulting gene contains the mouse apoE promoter with the mouse apoE being replaced by the human apoE so that only the human gene, and not the mouse gene, is expressed. The colony is maintained by homozygous breeding. To prevent genetic drift, regularly the human apoE mice expressing different isoforms are crossed with each other and subsequently again bred

to homozygosity to refresh the colony. Male and female mice that were homozygous for either apoE3 or apoE4 were studied by MTRA as described above. Two-way ANOVA used sex and *APOE* genotype as independent variables. As described above, T-Alb tissue/serum ratios were used to measure and correct for any BBB disruption.

Transport of I-S1 across iPSC-derived brain endothelial-like cells (iBECs)

The iBECs were derived from the GM25256 induced pluripotent stem cell (iPSC) line (Coriell Institute) using the method of Neal et al[58] with a seeding density of 15,000 cells per well for differentiation which was found to be optimal for this cell line. Use of this stem cell line was in accordance with an MTA between the VA Puget Sound Healthcare System and the Coriell institute, and was approved by the VA Puget Sound Healthcare System institutional biosafety committee. Briefly, iPSCs were grown to optimal density on plates coated with Matrigel (VWR cat no. 62405-134) in E8 Flex medium (Thermo Fisher Scientific cat no. A2858501), and then passaged using Accutase (Thermo Fisher Scientific cat no. A1110501) onto Matrigel-coated plates in E8 Flex medium plus 10 μM ROCK inhibitor Y-27632 (R&D Systems, cat no. 1254). The next day, the medium was changed to E6 (Thermo Fisher Scientific, cat no. A1516401) and E6 changes continued daily for 3 more days. Next, the medium was changed to human endothelial serum-free medium (HESFM, Thermo Fisher Scientific, cat no. 11111044) supplemented with 20 ng/mL bFGF (Peprotech, cat no. 100-18B), 10 μM retinoic acid (Sigma, cat no. R2625), and 1% B27 supplement (Thermo Fisher Scientific, cat no. 17504044). 48 h later, iBECs were subcultured onto 24-well transwell inserts (Corning cat no. 3470) coated with 1 mg/mL Collagen IV (Sigma, cat no. C5533) and 5mM Fibronectin (Sigma, cat no. F1141) in HESFM + 20 ng/mL bFGF, 10 uM retinoic acid, and 1% B27. 24 h after subculture, the medium was changed to HESFM + 1% B27 without bFGF or retinoic acid, and transendothelial electrical resistance (TEER) was recorded using an End EVOM2 Voltohmmeter (World Precision Instruments, Sarasota Florida) coupled to an ENDOHM cup chamber. TEER measurements occurred daily and S1 transport experiments were conducted when TEER stabilized, between 10–13 days in vitro.. TEER values in these studies exceeded 1000 $\Omega*cm^2$ and TEER means were confirmed to be equal among groups just prior to starting the transport study.

Prior to transport studies, the medium was changed and cells were equilibrated in the incubator for 20 min. Warm HESFM + 1% B27, 1 million CPM T-Alb, and 500,000 CPM of I-S1 was then added in a volume of 100 μL to the luminal chamber. After incubation times of 10, 20, 30, and 45 min at 37 °C, 500 μL volumes of medium from the abluminal chamber were collected and replaced with fresh pre-warmed medium. Samples were then acid precipitated by adding a final concentration of 1% BSA to visualize the pellet and 15% trichloroacetic acid to precipitate the proteins in solution. The samples were centrifuged at 4255xg for 15 min at 4 °C. Radioactivity in the pellet was counted in the gamma counter and the permeability-surface area coefficients for T-Alb and I-S1 were calculated according to the method of Dehouck et al[59]. Clearance was expressed as microliters (μL) of radioactive tracer that was transported from the luminal to abluminal chamber, and was calculated from the initial level of acid-precipitable radioactivity added to the luminal chamber and the final level of radioactivity in the abluminal chamber:

$$\text{Clearance } (\mu L) = [C]_C \times V_C / [C]_L \quad (5)$$

Where $[C]_L$ is the initial concentration of radioactivity in the luminal chamber (in units of CPM/μL), $[C]_C$ is the concentration of radioactivity in the abluminal chamber (in units of CPM/μL) and Vc is the volume of the abluminal chamber in μL. The volume cleared was plotted vs. time, and the slope was estimated by linear regression. The slopes of clearance curves for the iBEC monolayer plus Transwell® membrane was denoted by PS_{app}, where PS is the permeability × surface area product (in μL/min). The slope of the clearance curve for a Transwell® membrane without iBECs was denoted by $PS_{membrane}$. The PS value for the iBEC monolayer (PS_e) was calculated from $1 / PS_{app} = 1 / PS_{membrane} + 1 / PS_e$. The PS_e values were divided by the surface area of the Transwell® inserts (0.33 cm^2) to generate the endothelial permeability coefficient (Pe, in μL/min/cm^2).

Statistics and reproducibility

Sample size, randomization, and blinding: Sample sizes were pre-determined based on the variance that is known from previously conducting similar experiments on BBB transport. We selected samples sizes to power at 0.8–0.9 based on 30–40% differences between means. Anesthetized mice were randomized between test groups by alternating their assignments. Transwells were assessed for TEER prior to experiments and assigned to groups in such a way that TEER values between groups had approximately equal means and variances. Blinding was not done for experiments or analysis because this knowledge is required to carry out experiments and analysis.

Data exclusion and replication: For multiple-time regression analysis, the method calls for exclusion of data points that contribute to non-linearity of the curve. Outliers whose exclusion improved the $r^2 \geq 0.2$ were excluded from analysis. Excluded points are noted in Figures 2 and 3 by filled circles and further explained in those figure legends. For ANOVAs and comparisons of means, the Grubbs outlier exclusion test (alpha < 0.05) was applied once to detect single outliers, and any outliers that were excluded by this method are stated in the Figure legends and their values provided. Each figure was generated as a single experimental replicate, with the exception of iPSC studies where S1 and albumin transport were compared in three independent experiments. However, use of T-Alb as an internal control for all experiments allowed us to track consistency between experiments with different designs based on its predictable tissue/serum ratios. Further, the I-S1 tissue-serum ratios taken at the same time points from different experiments may be compared, and agree well with each other, demonstrating a reproducible observation of I-S1 transport into the brain and other tissues.

Statistical analysis: The Prism 8.0 statistical software package was used for all statistical calculations (GraphPad Inc, San Diego, CA). Simple linear regression analysis was used to calculate slopes and intercepts, and the error terms for the slope and Y-intercept are the standard errors. As required by multiple-time regression analysis, only the linear portion of the slope was used to calculate Ki. ANCOVA was used to determine whether slopes and intercepts of two lines differed, and two-way ANOVA was used to determine effects of sex

and genotype on regression lines in the APOE mouse studies. Two-tailed t-tests were used to compare two means and one-way or two-way analysis of variance (ANOVA) followed by multiple comparisons testing were used when more than two means are compared. The statistical tests used are specified in all figure legends. Data distribution was assumed to be normal, but was not formally tested. However, all data points are shown with the mean and standard deviation. Additional information can be found in the Life Sciences Reporting Summary.

Extended Data

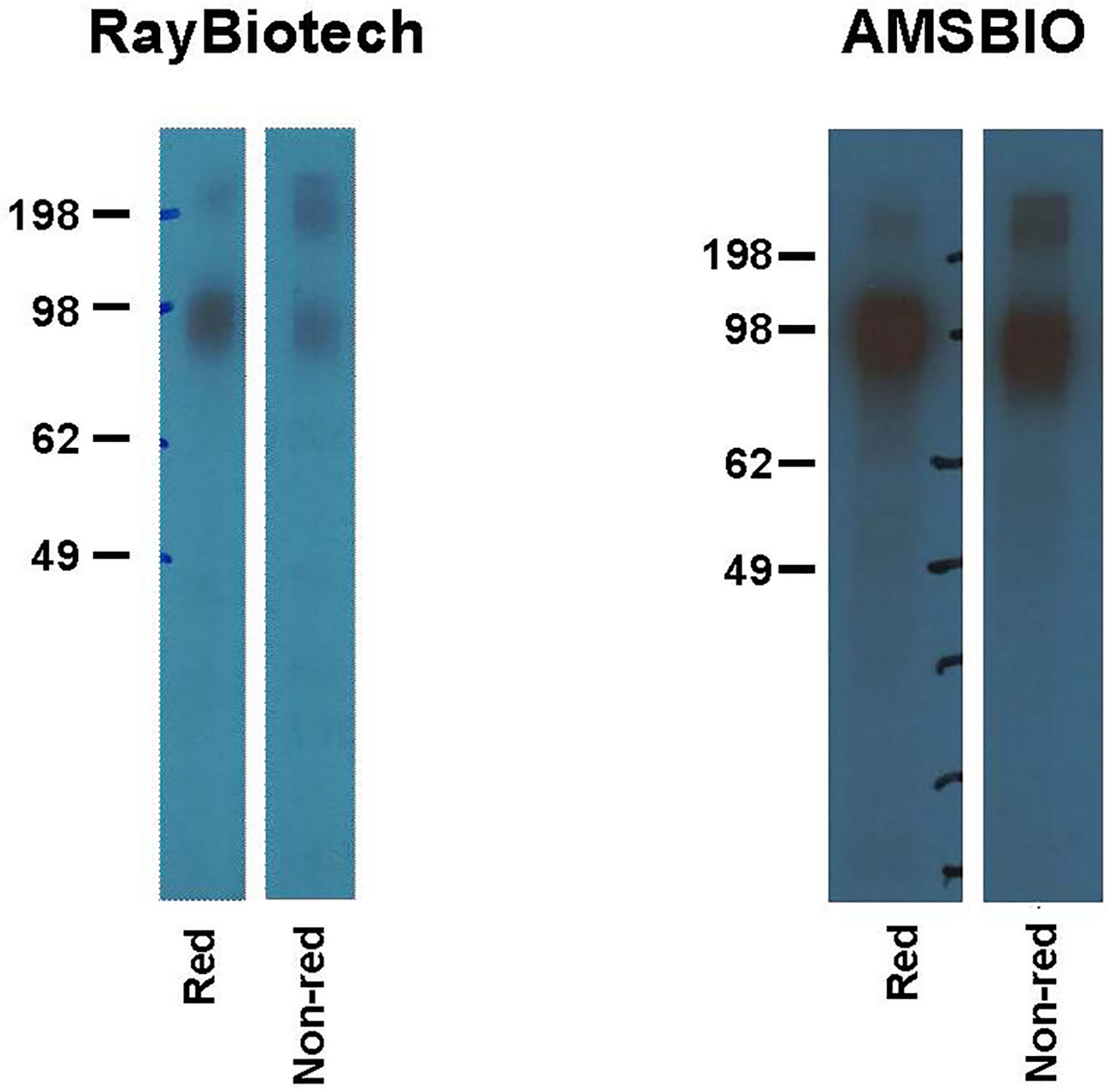

Extended Data Fig. 1.

Gel Autoradiography of I-S1 from RayBiotech and AMSBIO. Cropped images of Fraction 9 of I-S1 from RayBiotech (left panel,1μl of approximately 300,000 CPM run under reducing and non-reducing conditions, exposed to film for 24 hours), and from AMSBIO (right panel, 1μl of approximately 600,000 CPM run under reducing and non-reducing conditions). In each case, both the reduced and non-reduced gels migrated at the molecular weights predicted by the manufacturers. The autoradiography gels to validate size were run once. The quality of subsequent I-S1 labeling was confirmed by acid precipitation, described in methods.

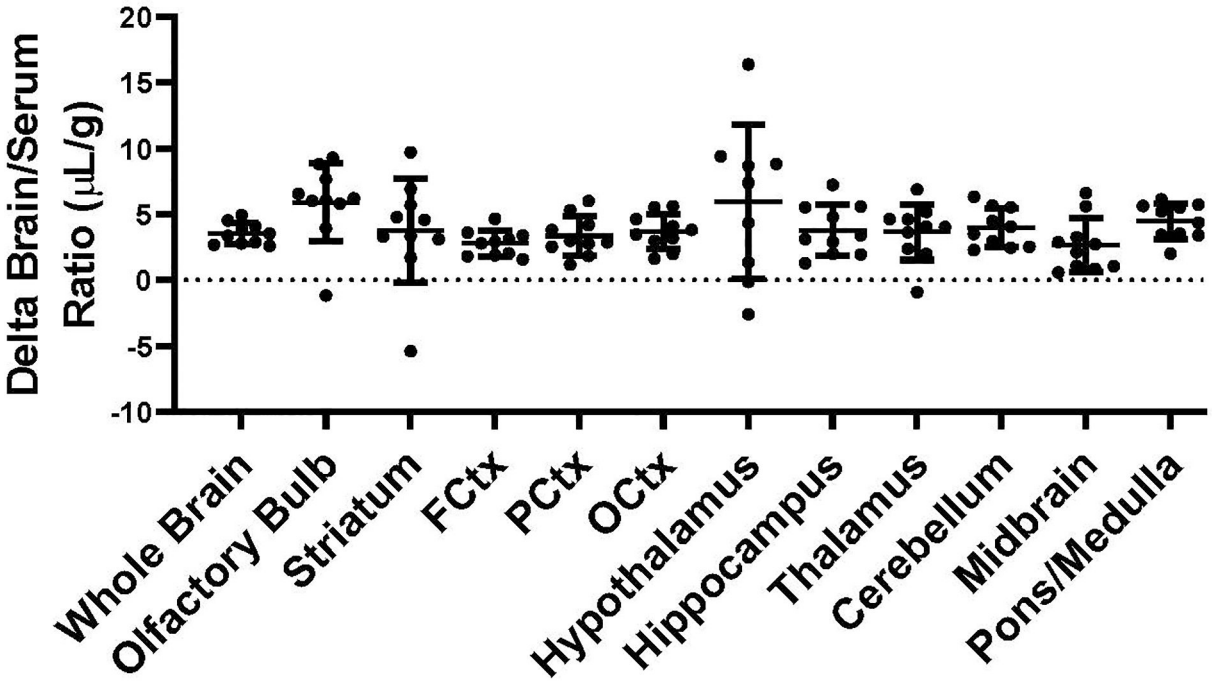

Extended Data Fig. 2.

I-S1 is uniformly taken up by all brain regions. Mice were given an injection of I-S1 (RayBiotech) and olfactory bulb, whole brain, and blood were collected 10 min later. Brains were dissected into the 10 regions shown. One-way ANOVA with brain regions as the independent variable showed a trend for differences ($p = 0.09$) and post-hoc multiple comparisons tests showed no differences among the brain regions. N = 11 mice. FCtx =frontal cortex, PCtx = parietal cortex, OCtx = occipital cortex.

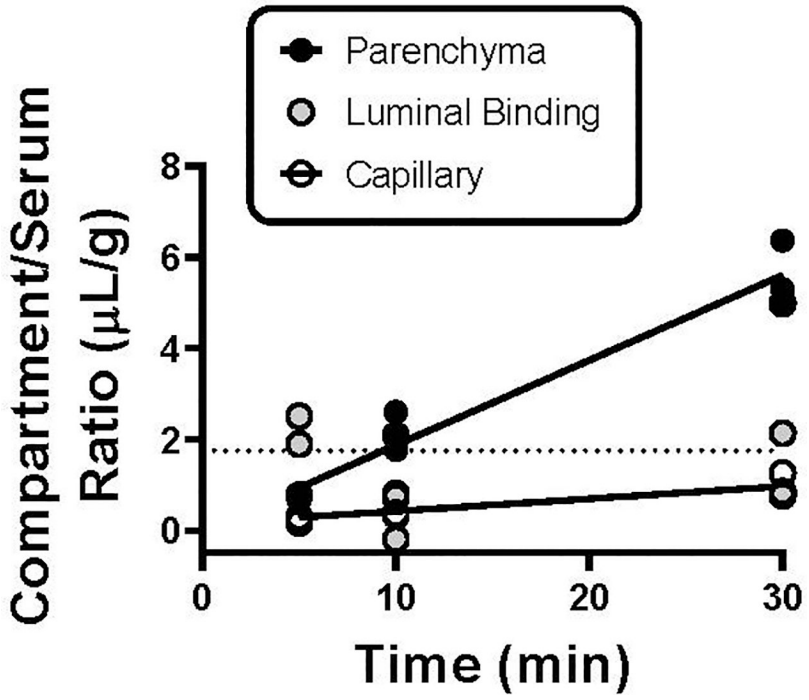

Extended Data Fig. 3.

Capillary depletion for I-S1. Capillary depletion studies were conducted to determine partitioning of the I-S1 (RayBiotech) in the capillary lumen, in the capillary, and in the brain parenchyma over time. The compartment that contained radioactivity was plotted against clock time, and the slopes were analyzed by linear regression. The slope of the line plotted for the parenchymal fraction was 0.187 ± 0.016 µL/g-min, r2 = 0.952, n = 9 mice, and was non-zero ($p < 0.0001$); the slope for the capillary fraction was 0.027 ± 0.006 µL/g-min, r2 = 0.757, n = 9 mice, and was non-zero ($p = 0.0023$). The slope for luminal binding was 0.05041 ± 0.04555 µL/g-min and did not significantly deviate from zero ($p = 0.3050$, n = 9, r2 = 0.145).The mean value for luminal binding over all time points was1.75 ± 0.50 µL/g.

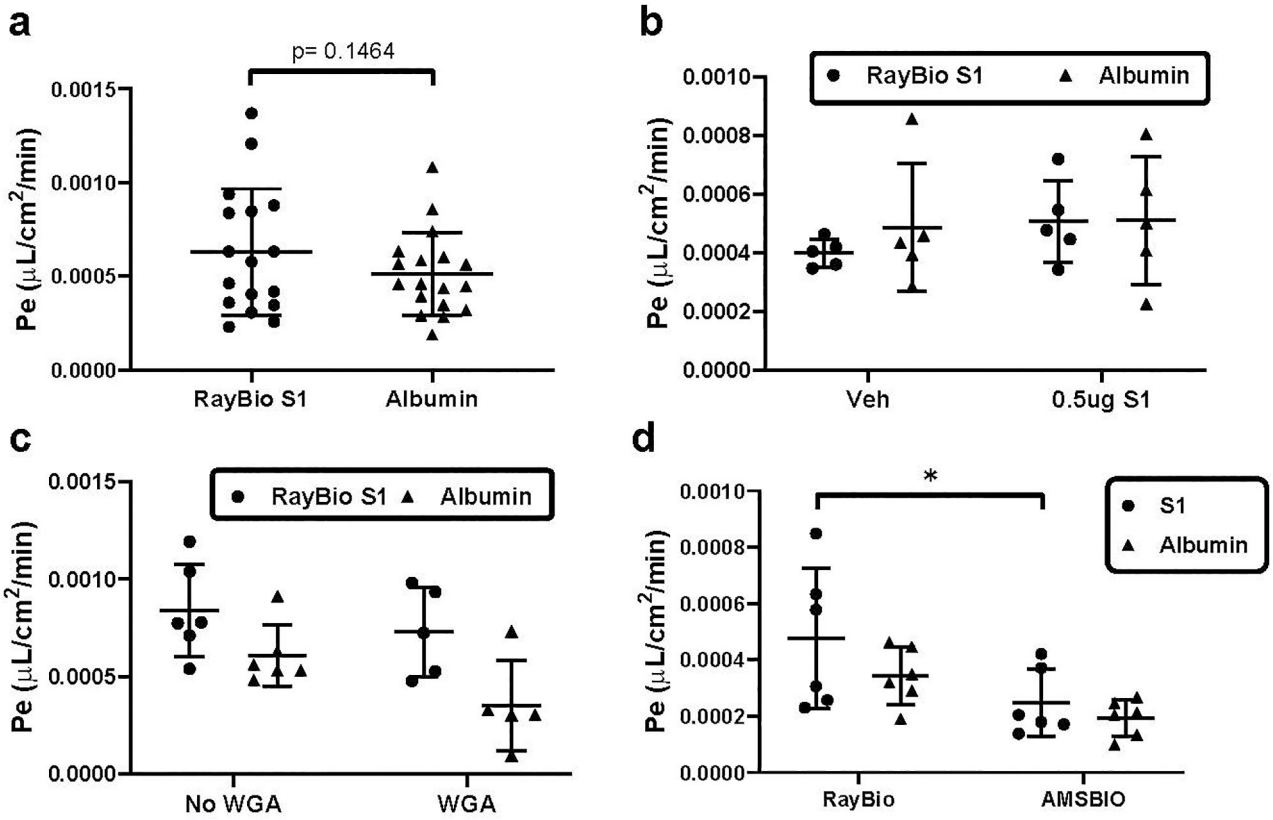

Extended Data Fig. 4.

Transport of S1 proteins across human iPSC-derived brain-like endothelial cell (iBEC) monolayers. **a**. RayBiotech I-S1 passage across the iBEC monolayer was not significantly faster than that of T-Alb ($p = 0.1464$, $t = 1.527$, $df=16$; two-tailed paired t-test). Combination of 3 independent differentiations, n = 17 transwells/group, average TEER (2578 ± 897.8 Ω*cm2). **b**. Transport of RayBiotech I-S1 in the presence of 5 μg/ml excess unlabeled S1. Excess S1 had no significant effect on I-S1 or T-Albumin Pe ($p > 0.5$; two-way ANOVA). N = 5–6 transwells/group from a single differentiation **c**. Transwells were treated with WGA (0.5 mg/ml) or vehicle. There was a significant overall effect of treatment ($F (1, 9) = 9.435$, $p = 0.0133$) and analyte ($F (1, 9) = 6.949$, $p = 0.0271$) on RayBiotech I-S1 or T-Alb transport (two-way ANOVA), but there were no significant effects of WGA on I-S1 or T-Alb Pe (Sidak's multiple comparisons testing). N = 5–6 wells/group from a single differentiation. **d**. Comparison of RayBiotech I-S1 and AMSBIO I-S1 transport. T-Alb was included with each I-S1 and also compared to the I-S1. Two-way ANOVA showed differences between I-S1s from the two sources) ($F(1,10) = 10.1$, $p = 0.0098$], but not between analytes (T-Alb vs I-S1). Multiple comparisons using Sidak's test showed a faster transport for RayBiotech I-S1 vs AMSBIO I-S1 ($p = 0.0324$). N = 6 wells/group from a single differentiation *$p < 0.05$.

Extended Data Table 1.

Stability as Assessed by Acid Precipitation of I-S1 in Brain and Blood 10 and 30 min after Intravenous Injection.

	10 min	30 min	Processing Control
Blood	98 ± 0.8	72 ± 1.8	94 ± 0.3
Brain	77 ± 0.04	24 ± 5.5	95 ± 0.2

Values are mean ± SE with units of percent (see equation 3); n = 3 for 10 min and 30 min and n = 2 for Processing Control.

Extended Data Table 2.

The number of mice used to calculate each regression line in figure 8 is shown here. Values in parentheses were excluded based on exclusion criteria for linear regression as described in methods.

	ApoE3 females	ApoE3 males	ApoE4 females	ApoE4 males
Brain (T-Alb)	11	10	10	10
Serum	11	9 (1)	9 (1)	10
Brain (I-S1)	11	9 (1)	9 (1)	10
Olfactory bulb	10 (1)	10	9 (1)	8 (2)
Lung	11	9 (1)	8 (2)	10
Liver	6 (5)	8 (2)	7 (3)	9 (1)
Spleen	7 (4)	8 (2)	9 (1)	9 (1)
Kidney	7 (4)	7 (3)	8 (2)	8 (2)

Supplementary Material

Refer to Web version on PubMed Central for supplementary material.

Acknowledgements

Supported by the VA (WAB, MAE), NIH R21 AG065928-01 (MAE), and NIH RF-1 AG059088 (WAB, JR).

We wish to thank Kristen Baumann, Riley Weaver, Sarah Pemberton, and Danny Quaranta for technical assistance.

Data availability:

The data that support the findings of this study are available from the corresponding author upon reasonable request.

References

1. Li YC, Bai WZ & Hashikawa T The neuroinvasive potential of SARS-CoV2 may play a role in the respiratory failure of COVID-19 patients. J Med Virol 92, 552–555 (2020). [PubMed: 32104915]
2. Mao L, et al. Neurologic Manifestations of Hospitalized Patients With Coronavirus Disease 2019 in Wuhan, China. JAMA Neurol 77, 1–9 (2020).
3. Saleki K, Banazadeh M, Saghazadeh A & Rezaei N The involvement of the central nervous system in patients with COVID-19. Rev Neurosci 31, 453–456 (2020). [PubMed: 32463395]

4. Moriguchi T, et al. A first Case of Meningitis/Encephalitis associated with SARS-Coronavirus-2. Int J Infect Dis 94, 55–58 (2020). [PubMed: 32251791]
5. Wang J, Jiang M, Chen X & Montaner LJ Cytokine storm and leukocyte changes in mild versus severe SARS-CoV-2 infection: Review of 3939 COVID-19 patients in China and emerging pathogenesis and therapy concepts. J Leukoc Biol 108, 17–41 (2020). [PubMed: 32534467]
6. Bleau C, Filliol A, Samson M & Lamontagne L Brain Invasion by Mouse Hepatitis Virus Depends on Impairment of Tight Junctions and Beta Interferon Production in Brain Microvascular Endothelial Cells. J Virol 89, 9896–9908 (2015). [PubMed: 26202229]
7. Subbarao K, et al. Prior infection and passive transfer of neutralizing antibody prevent replication of severe acute respiratory syndrome coronavirus in the respiratory tract of mice. J Virol 78, 3572–3577 (2004). [PubMed: 15016880]
8. Xu J, et al. Detection of severe acute respiratory syndrome coronavirus in the brain: potential role of the chemokine mig in pathogenesis. Clin Infect Dis 41, 1089–1096 (2005). [PubMed: 16163626]
9. Bullen CK, et al. Infectability of human BrainSphere neurons suggests neurotropism of SARS-CoV-2. Altex 37, 665–671 (2020). [PubMed: 32591839]
10. Erickson MA & Banks WA Neuroimmune axes of the blood-brain barriers and blood-brain interfaces: Bases for physiological regulation, disease states, and pharmacological interventions. Pharmacological Reviews 70, 278–314 (2018). [PubMed: 29496890]
11. Oh SK, et al. Identification of HIV-1 envelope glycoprotein in the serum of AIDS and ARC patients. Journal of Acquired Immune Deficiency Syndromes 5, 251–256 (1992). [PubMed: 1740750]
12. Westendorp MO, et al. Sensitization of T cells to CD95-mediated apoptosis by HIV-1 Tat and gp120. Nature 375, 497–500 (1995). [PubMed: 7539892]
13. Bansal AK, et al. Neurotoxicity of HIV-1 proteins gp120 and Tat in the rat striatum. Brain Research 879, 42–49 (2000). [PubMed: 11011004]
14. Rychert J, Strick D, Bazner S, Robinson J & Rosenberg E Detection of HIV gp120 in plasma during early HIV infection is associated with increased proinflammatory and immunoregulatory cytokines. AIDS Res Hum Retroviruses 26, 1139–1145 (2010). [PubMed: 20722464]
15. Banks WA, Kastin AJ & Akerstrom V HIV-1 protein gp120 crosses the blood-brain barrier: role of adsorptive endocytosis. Life Sciences 61, L119–L125 (1997).
16. Banks WA, Robinson SM & Nath A Permeability of the blood-brain barrier to HIV-1 Tat. Experimental Neurology 193, 218–227 (2005). [PubMed: 15817280]
17. Raber J, et al. Central nervous system expression of HIV-1 Gp120 activates the hypothalamic-pituitary-adrenal axis: evidence for involvement of NMDA receptors and nitric oxide synthase. Virology 226, 362–373 (1996). [PubMed: 8955056]
18. Banks WA, et al. Transport of human immunodeficiency virus type 1 pseudoviruses across the blood-brain barrier: role of envelope proteins and adsorptive endocytosis. Journal of Virology 75, 4681–4691 (2001). [PubMed: 11312339]
19. Banks WA, Robinson SM, Wolf KM, Bess JW Jr. & Arthur LO Binding, internalization, and membrane incorporation of human immunodeficiency virus-1 at the blood-brain barrier is differentially regulated. Neuroscience 128, 143–153 (2004). [PubMed: 15450361]
20. Weiss SR & Navas-Martin S Coronavirus pathogenesis and the emerging pathogen severe acute respiratory syndrome coronavirus. Microbiol Mol Biol Rev 69, 635–664 (2005). [PubMed: 16339739]
21. Yan R, et al. Structural basis for the recognition of SARS-CoV-2 by full-length human ACE2. Science 367, 1444–1448 (2020). [PubMed: 32132184]
22. Hoffmann M, et al. SARS-CoV-2 Cell Entry Depends on ACE2 and TMPRSS2 and Is Blocked by a Clinically Proven Protease Inhibitor. Cell 181, 271–280.e278 (2020). [PubMed: 32142651]
23. Shang J, et al. Structural basis of receptor recognition by SARS-CoV-2. Nature 581, 221–224 (2020). [PubMed: 32225175]
24. Villegas JC & Broadwell RD Transcytosis of protein through the mammalian cerebral epithelium and endothelium: II. Adsorptive transcytosis of WGA-HRP and the blood-brain and brain-blood barriers. Journal of Neurocytology 22, 67–80 (1993). [PubMed: 7680372]

25. Schweighardt B & Atwood WJ Virus receptors in the human central nervous system. Journal of Neurovirology 7, 187–195 (2001). [PubMed: 11517393]
26. Ramos-Kuri M, Barron Romero BL & Aguilar-Setien A Inhibition of three alphaherpesviruses (herpes simplex 1 and 2 and pseudorabies virus) by heparin, heparan and other sulfated polyelectrolytes. Archives of Medical Research 27, 43–48 (1996). [PubMed: 8867366]
27. Nottet HS, et al. Mechanisms for the transendothelial migration of HIV-1-infected monocytes into brain. The Journal of Immunology 156, 1284–1295 (1996). [PubMed: 8558009]
28. Banks WA, Kastin AJ, Brennan JM & Vallance KL Adsorptive endocytosis of HIV-1gp120 by blood-brain barrier is enhanced by lipopolysaccharide. Experimental Neurology 156, 165–171 (1999). [PubMed: 10192787]
29. Erickson MA & Banks WA Cytokine and chemokine responses in serum and brain after single and repeated injections of lipopolysaccharide: Mutliplex quantification with path analysis. Brain, Behavior, & Immunity 25, 1637–1648 (2011).
30. van Riel D, Verdijk R & Kuiken T The olfactory nerve: a shortcut for influenza and other viral diseases into the central nervous system. J Pathol 235, 277–287 (2015). [PubMed: 25294743]
31. Kuo CL, et al. ApoE e4e4 genotype and mortality with COVID-19 in UK Biobank. J Gerontol A Biol Sci Med Sci (2020).
32. Gebhard C, Regitz-Zagrosek V, Neuhauser HK, Morgan R & Klein SL Impact of sex and gender on COVID-19 outcomes in Europe. Biol Sex Differ 11, 29 (2020). [PubMed: 32450906]
33. Li LQ, et al. COVID-19 patients' clinical characteristics, discharge rate, and fatality rate of meta-analysis. J Med Virol 92, 577–583 (2020). [PubMed: 32162702]
34. Walls AC, et al. Tectonic conformational changes of a coronavirus spike glycoprotein promote membrane fusion. Proc Natl Acad Sci U S A 114, 11157–11162 (2017). [PubMed: 29073020]
35. McCray PB Jr., et al. Lethal infection of K18-hACE2 mice infected with severe acute respiratory syndrome coronavirus. J Virol 81, 813–821 (2007). [PubMed: 17079315]
36. Dohgu S, Ryerse JS, Robinson SM & Banks WA Human immunodeficiency virus-1 uses the mannose-6-phosphate receptor to cross the blood-brain barrier. PLoS One 7, e39565 (2012). [PubMed: 22761827]
37. Radzikowska U, et al. Distribution of ACE2, CD147, CD26 and other SARS-CoV-2 associated molecules in tissues and immune cells in health and in asthma, COPD, obesity, hypertension, and COVID-19 risk factors. Allergy 75, 2829–2845 (2020). [PubMed: 32496587]
38. Vankadari N & Wilce JA Emerging WuHan (COVID-19) coronavirus: glycan shield and structure prediction of spike glycoprotein and its interaction with human CD26. Emerg Microbes Infect 9, 601–604 (2020). [PubMed: 32178593]
39. Ibrahim IM, Abdelmalek DH, Elshahat ME & Elfiky AA COVID-19 spike-host cell receptor GRP78 binding site prediction. J Infect 80, 554–562 (2020). [PubMed: 32169481]
40. Guruprasad L Human coronavirus spike protein-host receptor recognition. Prog Biophys Mol Biol (2020).
41. Banks WA & Kastin AJ Characterization of lectin-mediated brain uptake of HIV-1 gp120. Journal of Neuroscience Research 54, 522–529 (1998). [PubMed: 9822162]
42. Hassanzadeh K, et al. Considerations around the SARS-CoV-2 Spike Protein with particular attention to COVID-19 brain infection and neurological symptoms. ACS Chem Neurosci (2020).
43. Prabakaran P, Xiao X & Dimitrov DS A model of the ACE2 structure and function as a SARS-CoV receptor. Biochem Biophys Res Commun 314, 235–241 (2004). [PubMed: 14715271]
44. Li X, et al. Risk factors for severity and mortality in adult COVID-19 inpatients in Wuhan. J Allergy Clin Immunol 146, 110–118 (2020). [PubMed: 32294485]
45. Machado C, DeFina PA, Chinchilla M, Machado Y & Machado Y Brainstem Dysfunction in SARS-COV-2 Infection can be a Potential Cause of Respiratory Distress. Neurol India 68, 989–993 (2020). [PubMed: 33109839]
46. Al-Ahmad AJ Comparative study of expression and activity of glucose transporters between stem cell-derived brain microvascular endothelial cells and hCMEC/D3 cells. Am J Physiol Cell Physiol 313, C421–c429 (2017). [PubMed: 28993322]

47. Lippmann ES, et al. Derivation of blood-brain barrier endothelial cells from human pluripotent stem cells. Nat Biotechnol 30, 783–791 (2012). [PubMed: 22729031]

48. Rodriguez GA, Burns MP, Weeber EJ & Rebeck GW Young APOE4 targeted replacement mice exhibit poor spatial learning and memory, with reduced dendritic spine density in the medial entorhinal cortex. Learn Mem 20, 256–266 (2013). [PubMed: 23592036]

49. Montelaro RC & Rueckert RR On the use of chloramine-T to iodinate specifically the surface proteins of intact enveloped viruses. J.Gen.Virol 29, 127–131 (1975). [PubMed: 171334]

50. Wang YF, Chuang MH, Chiu JS, Cham TM & Chung MI On-site preparation of technetium-99m labeled human serum albumin for clinical application. Tohoku J Exp Med 211, 379–385 (2007). [PubMed: 17409678]

51. Blasberg RG, Fenstermacher JD & Patlak CS Transport of alpha-aminoisobutyric acid across brain capillary and cellular membranes. Journal of Cerebral Blood Flow and Metabolism 3, 8–32 (1983). [PubMed: 6822623]

52. Blasberg RG, Patlak CS & Fenstermacher JD Selection of experimental conditions for the accurate determination of blood-brain transfer constants from single-time experiments: a theoretical analysis. Journal of Cerebral Blood Flow and Metabolism 3, 215–225 (1983). [PubMed: 6841469]

53. Triguero D, Buciak J & Pardridge WM Capillary depletion method for quantification of blood-brain barrier transport of circulating peptides and plasma proteins. Journal of Neurochemistry 54, 1882–1888 (1990). [PubMed: 2338547]

54. Gutierrez EG, Banks WA & Kastin AJ Murine tumor necrosis factor alpha is transported from blood to brain in the mouse. Journal of Neuroimmunology 47, 169–176 (1993). [PubMed: 8370768]

55. Knouff C, et al. Apo E structure determines VLDL clearance and atherosclerosis risk in mice. J Clin Invest 103, 1579–1586 (1999). [PubMed: 10359567]

56. Sullivan PM, et al. Targeted replacement of the mouse apolipoprotein E gene with the common human APOE3 allele enhances diet-induced hypercholesterolemia and atherosclerosis. J Biol Chem 272, 17972–17980 (1997). [PubMed: 9218423]

57. Siegel JA, Haley GE & Raber J Apolipoprotein E isoform-dependent effects on anxiety and cognition in female TR mice. Neurobiol Aging 33, 345–358 (2012). [PubMed: 20400205]

58. Neal EH, et al. A Simplified, Fully Defined Differentiation Scheme for Producing Blood-Brain Barrier Endothelial Cells from Human iPSCs. Stem Cell Reports 12, 1380–1388 (2019). [PubMed: 31189096]

59. Dehouck MP, et al. Drug transfer across the blood-brain barrier: correlation between in vitro and in vivo models. J Neurochem 58, 1790–1797 (1992). [PubMed: 1560234]

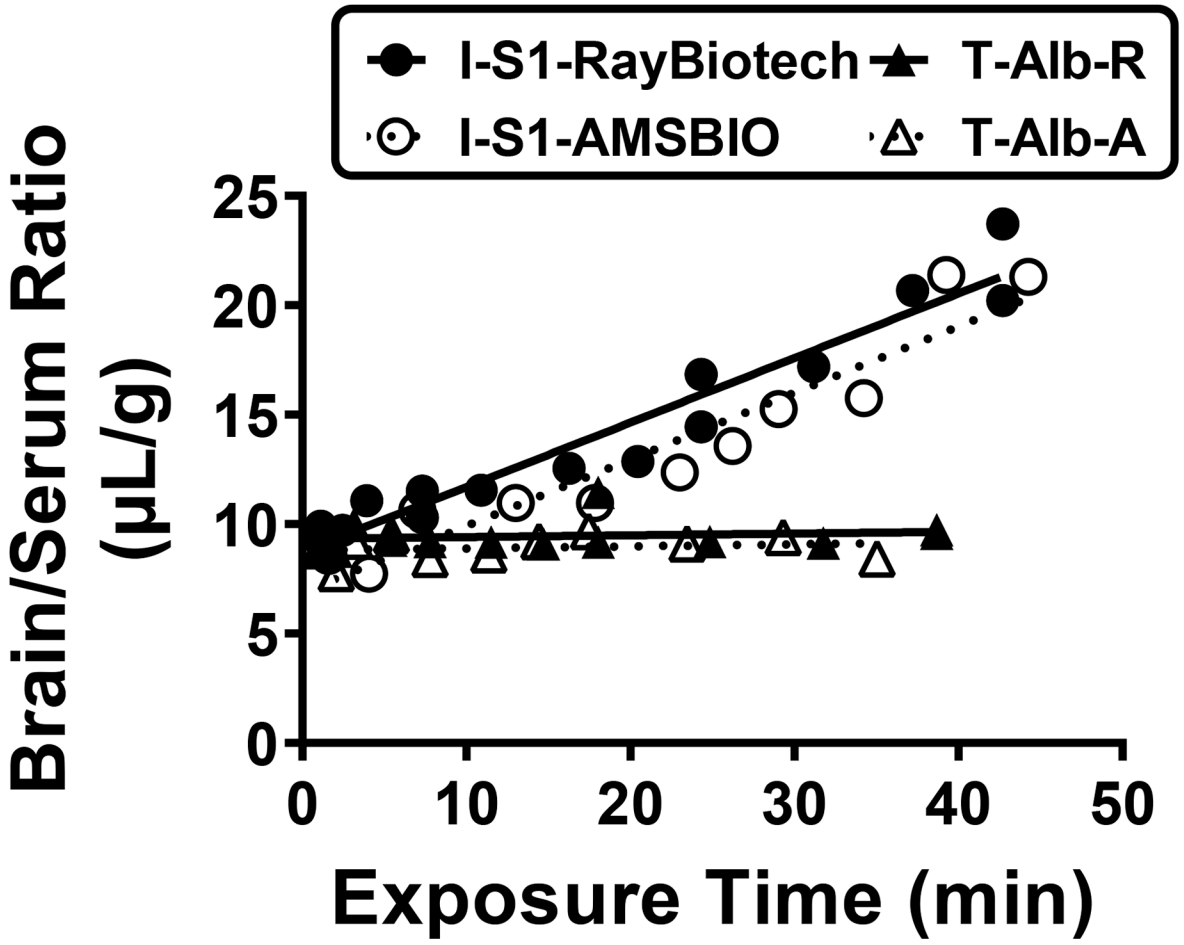

	Ki (µl/g-min)	Vi (µl/g)	r^2
I-S1 (RayBiotech)	0.295 ± 0.022	8.74 ± 0.50	0.935
I-S1 (AMSBIO)	0.304 ± 0.033	6.88 ± 0.84	0.905
T-Alb (RayBiotech)	0.00800 ± 0.0134	9.332 ± 0.263	0.0266
T-Alb (AMSBIO)	0.00941 ± 0.0164	8.798 ± 0.287	0.0355

Figure 1. S1 proteins from two commercial sources, RayBiotech and AMSBIO, are transported across the mouse BBB.

The brain/serum ratios of I-S1 from RayBiotech (I-S1-RayBiotech, filled circles) and AMSBIO (I-S1-AMSBIO, open circles) and T-Alb that was co-injected with I-S1-RayBiotech (T-Alb-R, filled triangles) or I-S1-AMSBIO (T-Alb-A, open triangles) are plotted against exposure time. The slopes of the lines represent the unidirectional influx rate (Ki) of each compound in units of µl/g-min, as described in methods. The Y-intercept (Vi) of each compound reflects the vascular space, and is expressed in µl/g. The Ki and Vi were calculated by simple linear regression. The Ki for I-S1 (RayBiotech) was significantly non-zero ($p<0.0001$), indicating that there was brain uptake; The Ki for I-S1 (AMSBIO)

was also significantly non-zero ($p<0.0001$). Statistical comparisons of I-S1 curves from each vendor showed no statistical difference between the Ki values: $F(1,22)=0.05881$, $p=0.8106$, but did show a difference between the Vi values: $F(1,23) = 10.32$, $p = 0.0039$. The Ki for T-Alb-R did not significantly deviate from zero ($p= 0.3556$), indicating that there was no brain uptake. The Ki for T-Alb-A also did not significantly deviate from zero, ($p= 0.5792$). The apparent lack of T-Alb brain uptake indicates that T-Alb remained confined to the vascular space and did not leak

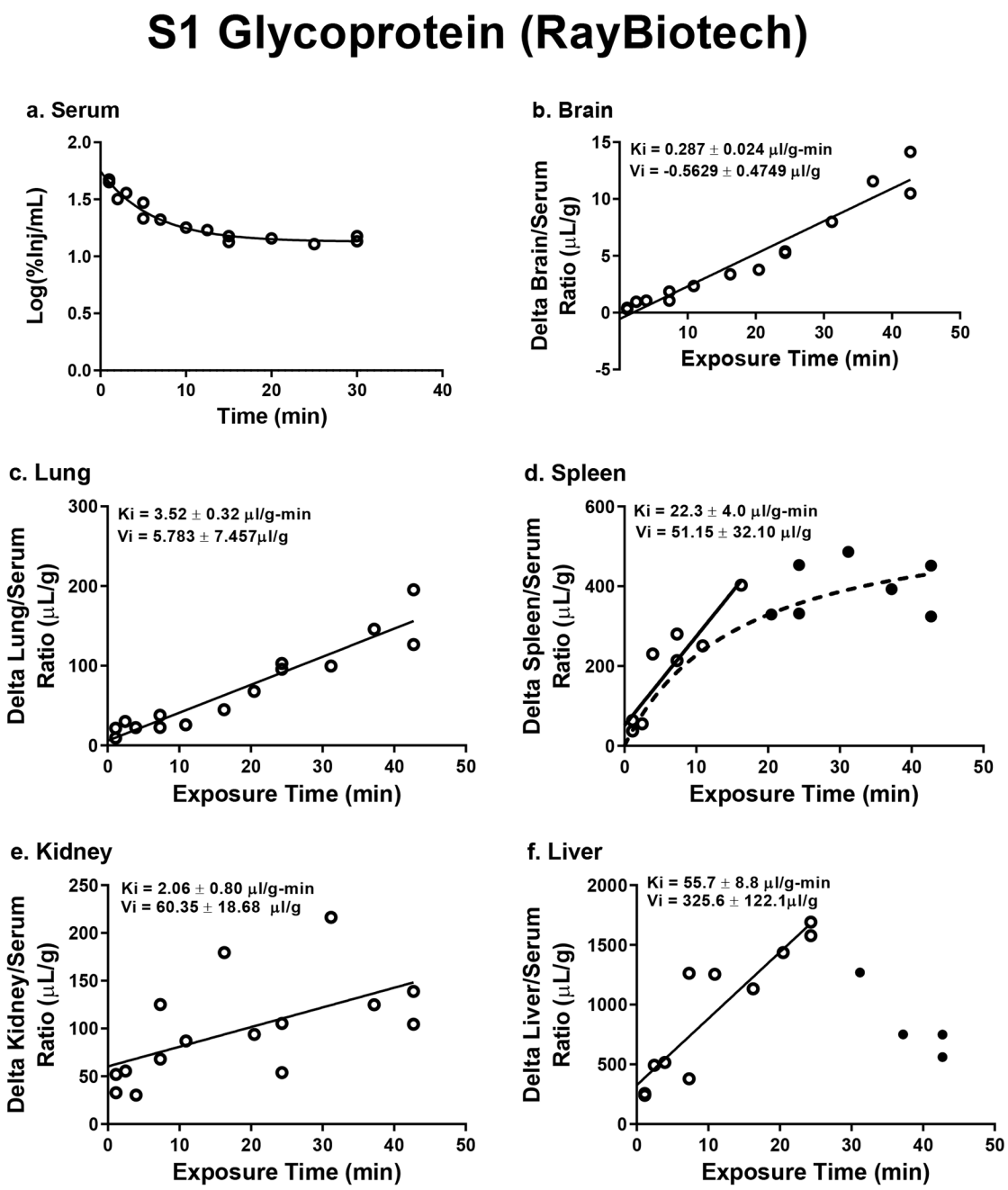

Figure 2. I-S1 (RayBiotech) is cleared from blood and taken up by peripheral tissues.

Panel **a.** Clearance of I-S1 from RayBiotech from blood, fitted to a nonlinear one phase exponential decay model: $Y = 0.617(e^{-0.165t}) + 1.13$ with a half-life = 4.20 min, n = 15 mice, $r^2 = 0.956$. Clearance from blood was linear for the first 10 min, with a half-time clearance of 6.6 min. **b-f.** The Y-axes show the delta tissue/serum ratios for I-S1, corrected for vascular space and non-specific leakage, as described in methods. **b.** The I-S1 Ki for whole brain was significantly non-zero ($p<0.0001$), indicating that there was tissue uptake (n=15 mice). **c-f.** These panels show the I-S1 Ki for different tissues calculated based on the linear portions of their curves. **c.** The I-S1 Ki for lung was significantly non-zero ($p<0.0001$) (n=15 mice).

d. The I-S1 Ki for spleen Ki was significantly non-zero ($p = 0.0014$) ($n = 8$ mice; 7 mice, shown as filled circles, were excluded from regression analysis due to non-linearity which violates assumptions of MTRA). **e.** The I-S1 Ki for kidney was significantly non-zero ($p = 0.024$) ($n=15$ mice). **f.** The I-S1 Ki for liver Ki was significantly non-zero ($p = 0.0001$) ($n = 11$ mice; 4 mice, shown as filled circles, were excluded from regression analysis because their inclusion caused non-linearity). All error terms are the standard error of the mean.

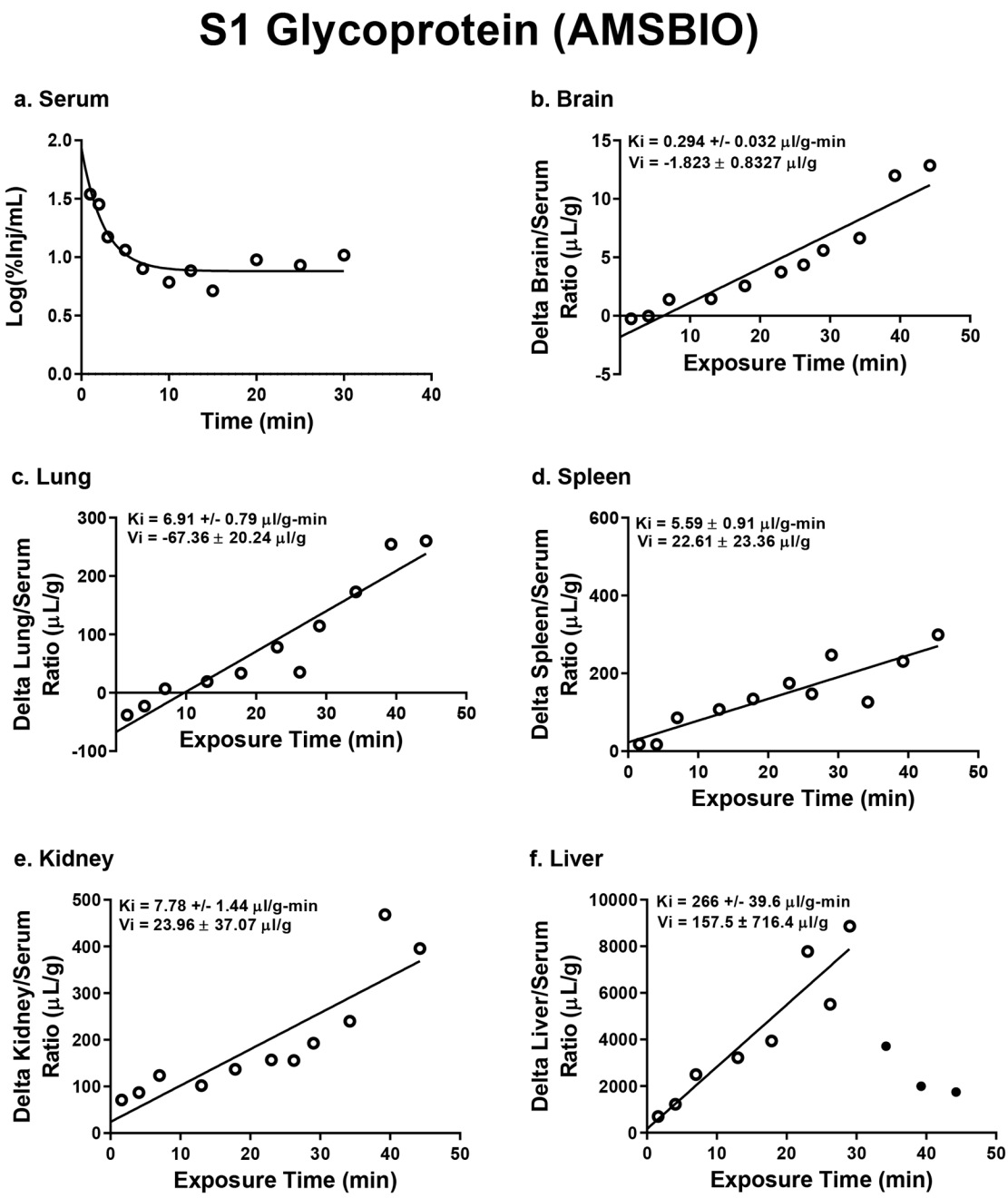

Figure 3. I-S1 (AMSBIO) is cleared from blood and taken up by peripheral tissues.

a. Clearance of I-S1 from AMSBIO from blood, fitted to a one phase exponential decay model, $Y = 1.05(e^{-0.393t})+ 0.880$, half life = 1.74 min, n = 11 mice, $r^2 = 0.867$. Clearance from blood was linear for the first 10 min, with a half-time clearance of 3.6 min. In panels **b-f**, the Y-axes show the delta tissue/serum ratios for I-S1, corrected for vascular space and non-specific leakage, as described in methods. **b.** The I-S1 Ki for whole brain was significantly non-zero ($p<0.0001$), indicating that there was tissue uptake (n=11 mice). **c-f.** These panels show the I-S1 Ki for different tissues calculated based on the linear portions of their curves. **c.** The I-S1 Ki for lung was significantly non-zero ($p<0.0001$, n=11 mice). **d.**

The I-S1 Ki for spleen was significantly non-zero ($p = 0.002$, n=11 mice). **e.** The I-S1 Ki for kidney spleen was significantly non-zero ($p = 0.0004$, n=11 mice). **f.** The I-S1 Ki for liver was significantly non-zero ($p = 0.0005$; n = 8 mice (3 mice, shown as filled circles, were excluded from regression analysis because their inclusion caused non-linearity)). All error terms are the standard error of the mean.

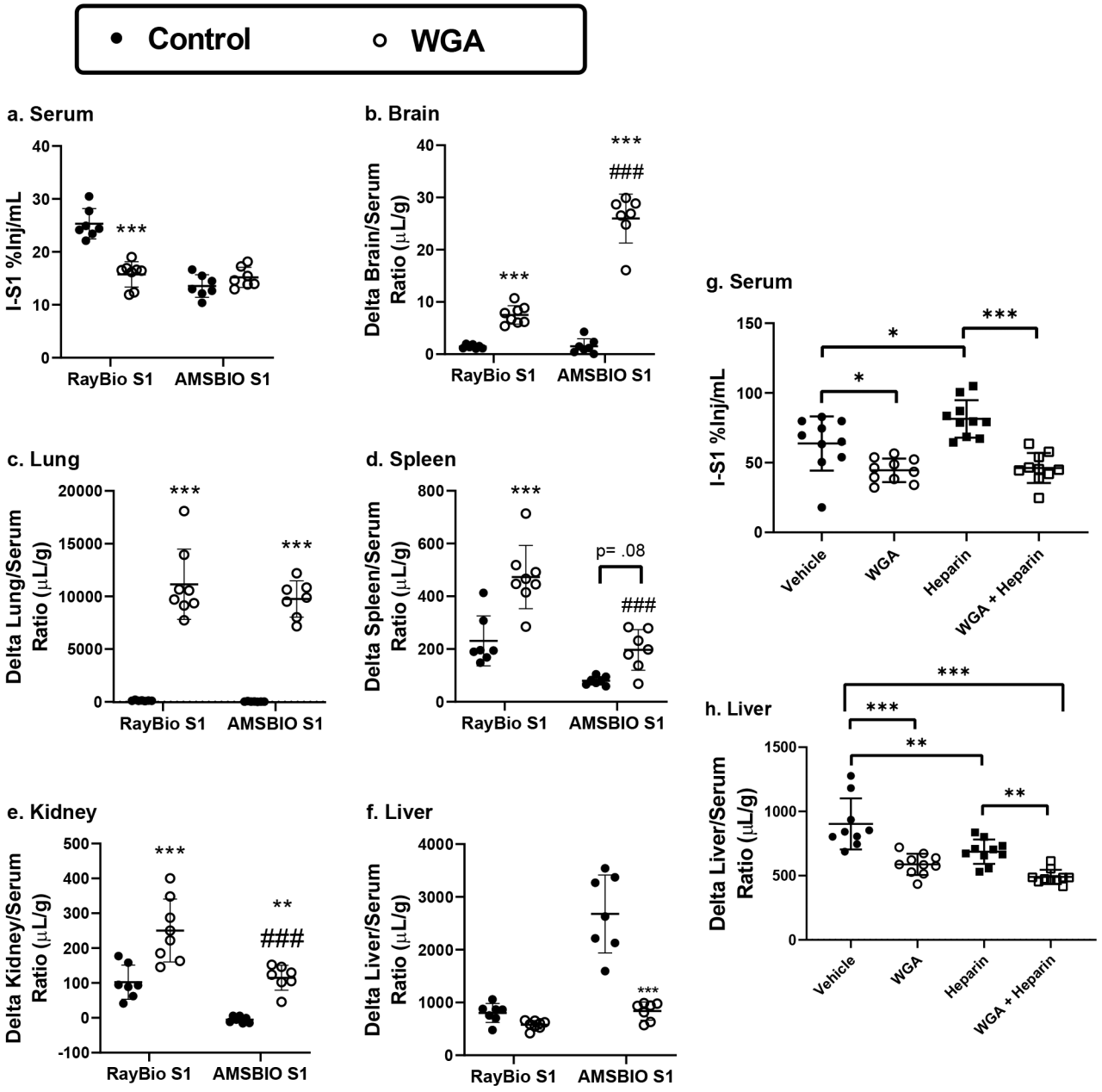

Figure 4. WGA treatment enhances I-S1 uptake by brain, lung, spleen, and kidney and heparin blocks uptake by liver.

Panels **a-f** show serum levels and tissue uptake of radioiodinated S1 from either RayBiotech or AMSBIO 10 min after intravenous injection in which WGA, a stimulator of adsorptive transcytosis, was included in the injections to half the mice. **a.** Serum I-S1 levels expressed as the percent of the injected dose per ml of serum. There was a main effect of S1 source ($F(1, 25) = 49.79$, $p<0.0001$) and treatment ($F(1, 25) = 20.57$, $p<0.0001$), as well as a significant effect of their interaction ($F(1, 25) = 40.93$, $p<0.0001$). WGA treatment decreased I-S1 (RayBiotech) levels in serum ($p<0.0001$), indicating increased clearance from blood. **b.** Brain I-S1 levels expressed as delta brain/serum ratios, showing significant effects (all $p<0.0001$) of S1 source ($F(1, 25) = 92.98$), treatment ($F(1, 25) = 252.2$), and

their interaction (F (1, 25) = 91.41). These results show that WGA stimulated I-S1 uptake from both RayBiotech and AMSBIO and that WGA stimulated uptake of S1 from AMSBIO more than from RayBiotech. **c.** Lung I-S1 levels show an effect of treatment (F (1, 25) = 204.6, p<0.0001). **d.** Spleen I-S1 levels show effects of S1 source (F (1, 25) = 43.06, p<0.0001) and treatment (F (1, 25) = 30.42, p<0.0001), and a trend for interaction (F (1, 25) = 3.657, p = 0.08). **e.** Kidney I-S1 levels show effects of source (F (1, 25) = 33.45, P<0.0001) and treatment (F (1, 25) = 40.77, p<0.0001). **f.** Liver I-S1 levels show effects of source of S1 (F (1, 25) = 55.87), treatment (F (1, 25) = 52.16) and their interaction (F (1, 25) = 32.08), all at p<0.0001. For **a-f** data were analyzed using two-way ANOVA with S1 source (RayBiotech vs AMSBIO) and treatment (with or without WGA) as main factors, followed by Tukey's multiple comparisons tests; figures show mean and standard deviation. *p<0.05, **p<0.01, and ***p<0.001 indicating comparisons of treatments within I-S1 group (RayBiotech or AMSBIO); #p<0.05, ##p<0.01, ###p<0.001 indicating comparisons of I-S1 groups within treatments. N = 7/group, except for Raybio S1-WGA mice (n-=8).
Panels **g-h** show serum levels and liver uptake of radioiodinated S1 from RayBiotech 10 min after intravenous injection with or without co-injection of WGA, heparin or both. **g.** Heparin increased serum levels of I-S1 (p = 0.016), but did not block the effect of WGA on I-S1 serum levels. **h.** In comparison to vehicle, uptake of I-S1 was decreased by heparin (p = 0.0015), WGA (p<0.0001), and WGA + heparin (p<0.001). Liver uptake of I-S1 was lower after WGA + heparin vs heparin alone (p = 0.0034) but not vs WGA alone. *p<0.05, **<0.01, ***<0.001. For **g-**h, data were analyzed by one-way ANOVA and Sidak's multiple comparisons test, and n=10 for each group, with the exception of liver vehicle in panel **h**, where one outlier was identified using a Grubbs test (77.6 ul/g) and excluded, leaving n=9 mice.

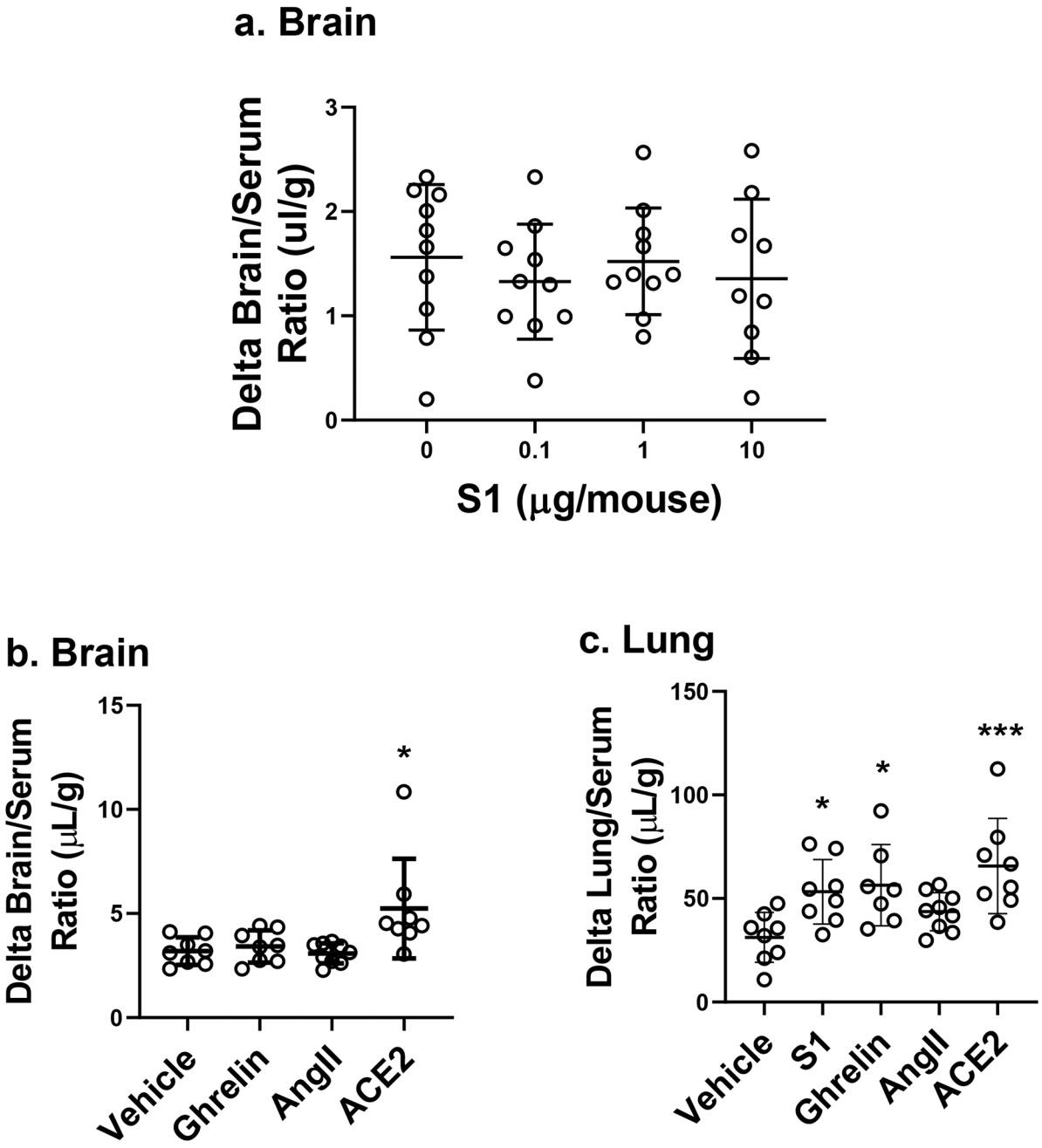

Figure 5. Effects of unlabeled S1, ACE2, and ACE2 substrates on I-S1 uptake into tissues.

Panels show tissue uptake of radioiodinated S1 from RayBiotech 10 min after intravenous injection with or without unlabeled S1 (from AMSBIO), ACE2 or the ACE2 substrates ghrelin or angiotensin II (Ang II). The Y-axis shows the albumin-corrected (delta) tissue/serum ratio, and the mean and standard deviation are shown. **a.** Unlabeled S1 at doses 0.1 ug (n-=10 mice), 1 ug (n=10 or 10 ug (n=9) did not reduce brain I-S1 uptake compared to vehicle controls (n=10) (One-way ANOVA: $F(3,33)=0.6312$, $p = 0.6$). **b.** Co-injection had a significant main effect on brain I-S1 uptake (one-way ANOVA $F(3,29) = 4.7$, $p = 0.0073$), with 1μg ACE2 increasing uptake (ACE2 vs. vehicle, p=0.0109 (Dunnett's multiple

comparisons test) but no effect of 1μg ghrelin or 1μg AngII. *p<0.05. N= 8, 8, 9, and 8 for the vehicle, ghrelin, AngII, and ACE2 groups, respectively. **c.** Co-injection had a significant main effect on lung I-S1 uptake (one-way ANOVA $F(4, 35) = 5.12$, $p = 0.0023$), with significant effects of 1μg unlabeled S1 (p= 0.0372), 1μg ghrelin (p= 0.0188) and 1μg ACE2 (p= 0.0007), but no effects of 1μg AngII (p= 0.3511; all Dunnett's test). * p<0.05, ** p<0.01, *** p<0.001. N= 8, 8, 7, 9, and 8 for vehicle, S1, ghrelin, AngII, and ACE2, respectively. One outlier (201 μl/g) in the ghrelin group was detected by a Grubbs test (alpha <0.05) and excluded from analysis.

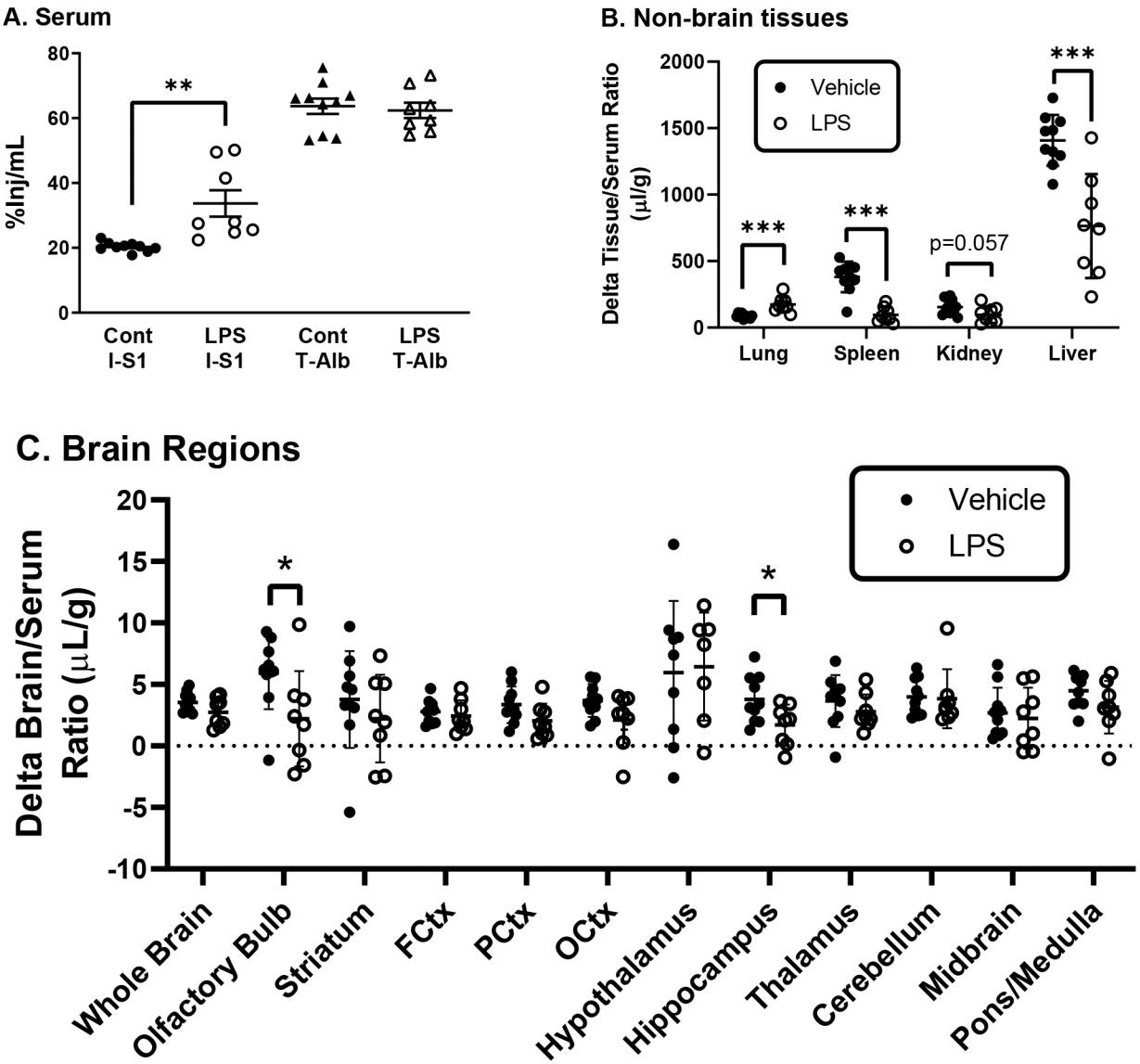

Figure 6. LPS has minimal effects on brain I-S1 uptake, but alters I-S1 clearance from blood and uptake by peripheral tissues.

We treated mice with intraperitoneal LPS using a protocol previously shown to alter BBB permeability and induce inflammation, as described in methods. Four hours after the last injection of LPS, we gave mice an intravenous injection containing I-S1 (RayBiotech) and T-Alb and collected tissue and blood samples 10 min after the intravenous injection. **a.** Serum levels of I-S1 (RayBiotech), expressed as % injected dose present in a ml of serum (%Inj/ml), were increased 4h after LPS injection vs control ((t = 3.66, df = 16, p = 0.0021, two-tailed t-test), indicating that LPS decreased clearance of I-S1 from blood. LPS had no significant effect on the serum levels of T-Alb (t= t=0.3739, df=16, p= 0.7134), indicating a selective effect of LPS on I-S1 clearance. **b.** Tissue levels of I-S1, expressed as tissue/serum ratios corrected (delta brain/tissue ratios) for vascular space and leakage by subtracting the tissue/serum ratios for T-Alb. LPS increase I-S1 uptake by lung (t = 4.58, df = 16, p = 0.0003) and decreased I-S1 uptake by spleen (t = 6.39, df = 16, p<0.0001) and liver (t =

4.60, df = 16, p = 0.0003); the effect of LPS on I-S1 uptake by kidney was not significant (p = 0.057) (all 2-tailed t-tests). The decreased I-S1 uptake by liver likely contributes to the decrease in I-S1 clearance from blood seen in panel **a**. **c.** Levels of I-S1 in brain areas, expresses as delta brain/serum ratios. Two-way ANOVA showed a significant main effect of brain region [F(11,190) = 2.72, p = 0.0028] accounting for 12.5% of the variability, and a main effect of LPS treatment [F(11,190) = 10.7, p = 0.0012] accounting for 4.5% of the variability; there was no statistically significant effect for interaction. Sidak's multiple comparisons test showed that LPS treatment decreased I-S1 uptake by olfactory bulb (p = 0.026), but not other brain regions. * p<0.05, **<0.01, *** <0.001, and t = 0.1>p>0.05. FCtx = frontal cortex, PCtx = parietal cortex, OCtx = occipital cortex. Panels show mean and standard deviation. Control groups (panel **a**), n=10 mice; vehicle group (panels **b,c**) n=10 mice, LPS group (panels **a-c**) n=10 mice.

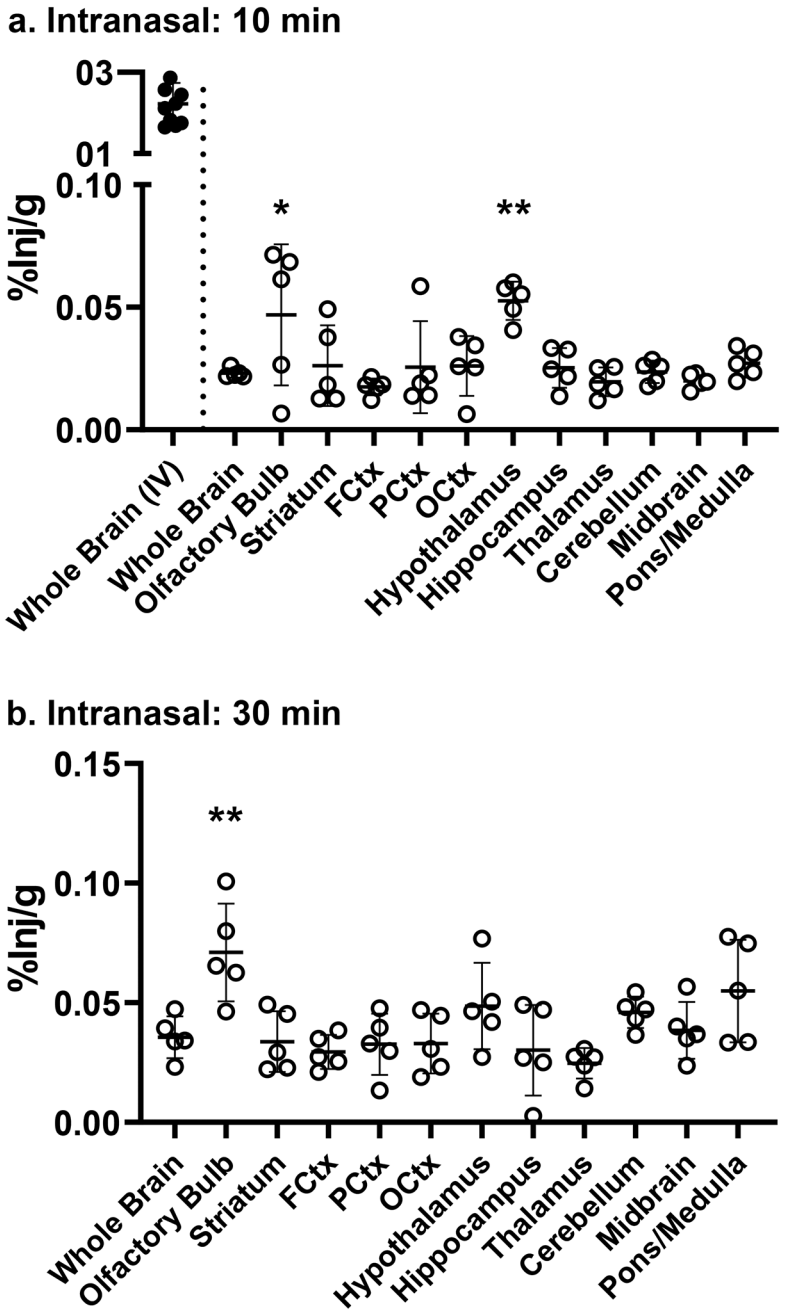

Figure 7. I-S1 enters the brain after intranasal administration.

Brain uptake of I-S1 (RayBiotech) delivered intranasally (1 μL/naris), expressed as % administered dose taken up per g of each brain region (%Inj/g). **a.** Ten minutes after intranasal administration, I-S1 was detected in all dissected brain regions. One-way ANOVA showed a significant effect of brain region [$F(11, 48) = 3.77$, $p = 0.0006$], with significantly higher uptake in olfactory bulb ($p = 0.031$) and hypothalamus ($p = 0.0041$) compared to whole brain (Dunnett's multiple comparisons test). Whole-brain uptake after intranasal administration was 0.023 ± 0.0008 %Inj/g; for visual comparison, the panel also shows the whole-brain %Inj/g 10 min after IV injection as calculated from the control values

for the LPS experiment in Figure 6 (filled circles, 0.22 ± 0.016 %Inj/g); N=5 mice. **b.** Thirty minutes after intranasal administration, I-S1 was detected in all dissected brain regions. One-way ANOVA showed a significant effect of brain region ($F(11,48) = 4.33$, $p = 0.0002$), with significantly more uptake in the olfactory bulb compared to whole brain ($p = 0.0023$, Dunnett's multiple comparisons test). A two-tailed t-test showed significant increases between 10 and 30 minutes for whole brain ($p=0.0143$, $t=3.116$, $df=8$), frontal cortex ($p=0.0391$, $t=2.464$, $df=8$), cerebellum ($p=0.0003$, $t=6.226$, $df=8$), midbrain ($p=0.0098$, $t=3.370$, $df=8$) and pons ($p=0.0232$, $t=2.801$, $df=8$) but not the other regions. N=5 mice. * $p<0.05$, ** <0.01, *** <0.001; FCtx = frontal cortex, PCtx = parietal cortex, OCtx = occipital cortex.

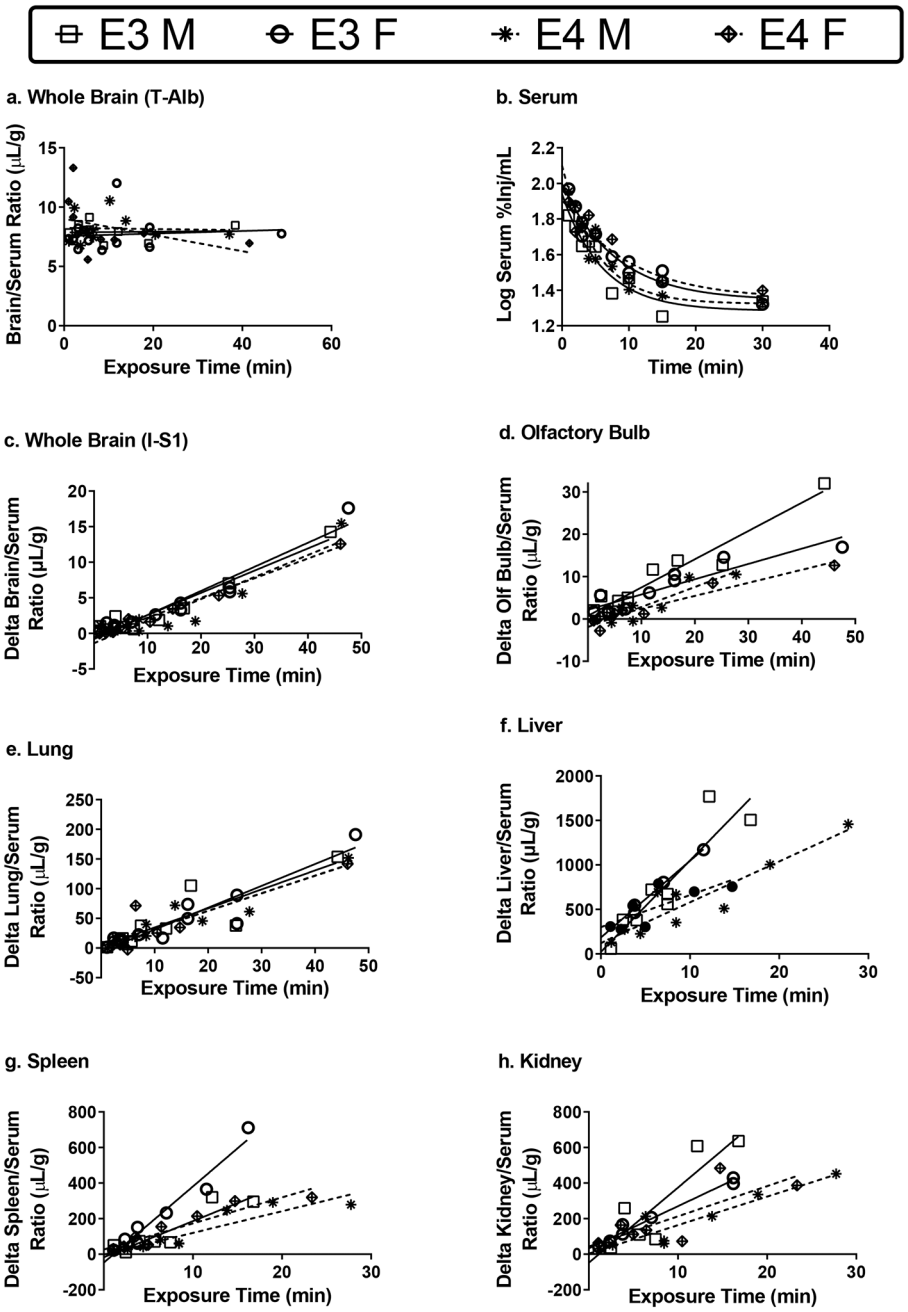

Figure 8. Sex and ApoE genotype influence on I-S1 uptake.

Serum levels and tissue uptake of I-S1 (RayBiotech) and brain uptake of T-Alb following intravenous injection in male and female mice that were homozygous for human *APOE3* (E3) or *APOE4* (E4). For panel **a**, multiple-time regression analysis was performed to calculate the Ki and Vi for T-Alb. Neither sex nor genotype affected clearance of I-S1 from blood (panel b). In panels **c-h**, the Y-axis shows delta tissue/serum ratios for I-S1, which are corrected for vascular space and non-specific leakage, as described in methods. The slopes of the regression lines that result from multiple-time regression analysis measures the rate of influx (Ki) into the tissues. The Ki values for the four groups (E3 males, E3 females,

E4 males, and E4 females) were statistically compared by two-way ANOVA with sex and *APOE* genotype as the independent variables, followed by Tukey's multiple comparison post-hoc tests in all panels. Ki values in figures are shown with their standard error of the mean. Sex or APOE genotype did not influence changes in brain uptake of T-Alb (**a**), levels of I-S1 in serum (**b**), or I-S1 uptake by brain (c) or lung (e) indicating that these factors do not influence BBB integrity or brain vascular space, clearance from blood, or uptake by brain or lung. **d.** Two-way ANOVA showed a significant effect of sex on I-S1 uptake in the olfactory bulb ($F(1, 29) = 14.30$, $p = 0.0007$), accounting for 29% of the variability. Post-hoc Tukey's multiple comparisons showed a significantly larger Ki for E3 males compared to E3 females ($p = 0.0056$) and to E4 females ($p = 0.0015$). APOE genotype had a trend-level effect on uptake in the olfactory bulb ($F(1, 29) = 3.838$, $p = 0.06$). **f.** *APOE* genotype had a significant main effect on I-S1 uptake in the liver ($F(1, 24) = 28.44$, $p<0.0001$) accounting for 50% of the variability, with a lower uptake rate for E4 females compared to E3 females ($p = 0.0057$) and to E3 males ($p = 0.0001$), and a lower uptake rate for E4 males vs E3 males ($p = 0.0039$). **g**: There was a significant main effect of sex on I-S1 uptake in the spleen ($p = 0.0004$) accounting for 20% of the variability, a main effect of ApoE genotype ($p<0.0001$) accounting for 43% of variability, and a significant effect of their interaction ($p= 0.0029$) accounting for 13% of variability. Multiple comparisons showed faster uptake rates for E3 females compared to E4 females ($p<0.0001$) to E3 males ($p = 0.0003$), and to E4 males ($p<0.0001$). **h**: *APOE* genotype had a significant effect on I-S1 uptake in the kidney ($p = 0.0046$) accounting for 25% of variability, with faster uptake in E3 males compared to E4 males ($p = 0.0089$) and to E4 females ($p = 0.012$). The number of mice assigned each group was 11 E3 females, and 10 for the other three groups. However, the N's used to calculate the regression lines ranged from 6–11 per group, because deviation from linearity was observed that satisfied exclusion criteria, as described in methods. The n per group (including the excluded outliers) is shown in Supplementary Table 2.